10-21-2021

# Forcespun polyvinylpyrrolidone/copper and polyethylene oxide/ copper composite fibers and their use as antibacterial agents

Md Toukir Hasan

Ramiro Gonzalez

Ari Alexis Munoz

Luis Materon

Jason Parsons

*See next page for additional authors*

Authors
Md Toukir Hasan, Ramiro Gonzalez, Ari Alexis Munoz, Luis Materon, Jason Parsons, and Mataz Alcoutlabi

Alcoutlabi Mataz (Orcid ID: 0000-0003-4641-9109)

# Forcespun PVP/Cu & PEO/Cu Composite fibers and their use as Antibacterial Agents

Md Toukir Hasan[1], Ramiro Gonzalez[1], Ari Alexis Munoz[2], Luis Materon[2], Jason. G. Parsons[3], Mataz Alcoutlabi[1, *]

[1]*Mechanical Engineering Department, University of Texas Rio Grande Valley, Edinburg, USA*

[3]*Department of Biology, University of Texas, Rio Grande Valley, Edinburg, Texas 78539*

[4]*Department of Chemistry University of Texas, Rio Grande Valley, 1 W University Blvd. Brownsville, Texas 78521, USA*

## Abstract

Cu nanoparticles (CuNPs) embedded in Polyvinylpyrrolidone (PVP) and Polyethylene Oxide (PEO) fiber-matrices were prepared through centrifugal spinning of PVP/ethanol and PEO/aqueous solutions, respectively. The prime focus of the current study is to investigate the antibacterial activity of composite fibers against Escherichia coli (*E. coli*) and Bacillus cereus (*B. cereus*) bacteria. During the fiber formation, the centrifugal spinning parameters such as spinneret rotational speed, spinneret to collector distance and relative humidity were carefully chosen to obtain long and continuous fibers. The structural and morphological analysis of both composite fibers were investigated using Scanning Electron Microscopy (SEM), X-Ray Diffraction (XRD), Energy-dispersive X-ray spectroscopy (EDS) and Thermo gravimetric Analysis (TGA). In the antibacterial test, PVP/Cu and PEO/Cu composite fibrous membranes exhibited inhibition efficiency of 99.98 % and 99.99 % against *E. coli* and *B. cereus* bacteria, respectively. Basically, CuNPs were well embedded in the fibrous membrane at the nanoscale level which facilitated the inhibition of bacterial functions through the inactivation of the chemical structure of the cells. Such an effective antibacterial agent obtained from forcespun composite fibers could be promising candidates for biomedical applications.

* Corresponding Author. Tel: 956-665-8945. Email: mataz.alcoutlabi@utrgv.edu

## Introduction

Nowadays, microorganism (e.g. *Gram positive* and *Gram negative* bacteria) originated from spoilage or contaminated products is rampantly affecting the compositional change of human intestine negatively [1, 2] by which the tissue interlink system can collapse [3]. Correspondingly, for the protection from microorganisms, efficacious antibacterial agents, developed from suitable metal/polymer nano-composites, have been widely used to impede bacterial cell proliferation due to having higher efficiency, stability, biocompatibility, biodegradability and availability to process [4-6]. Fortunately, human skin is coherently compatible with the morphological characteristics of nanofibrous membrane [7, 8], facilitating the inhibition of bacteria through absorbing exudates [9-11].

Nanotechnology promotes to develop nanofibers conveying high specific surface area to volume ratio, surface composition [12] and higher porosity with functional additives where the interfacial strength of layers is congruent to the size, shape, and composition of the nanofibers. In general, the antibacterial ability of a fibrous membrane is a variable function of the surface area in contact with the bacterial layers [13]. Conceptually, nanofibers react significantly with the bacterial surface because of their high surface area and porosity. Zupančič et al [14] reported that thicker nanofibers can reduce the bacterial cell mobility more profusely and quickly than thinner fibers as the response was cell-line specific [15, 16]. Therefore, nanofibers can exhibit strong inhibition performance and be used as antibacterial agents [17, 18] in drug delivery [19, 20], tissue engineering [21-23], bio-adhesive [20] and filtration

Nano/micro fibers can be prepared by various processing methods such as melt blowing, electrospinning [24-26], centrifugal spinning[27-34], dry spinning[35], phase separation[36] and self-assembly [37]. Centrifugal spinning or Forcespinning (FC) has been recently used to produce fibers at a high production rate (1g/min) and low cost [32, 33, 38] where both conducting and non-conducting solutions/melts can be centrifugally spun into fibers [29, 39]. Beyond these features, for an identical solution at ambient conditions, centrifugally spun fibers yield more porous-based shape than electrospun fibers [14, 40].

Several polymer systems have been recently centrifugally spun into fibers[41, 42]. Likewise, PEO and PVP polymers have been forcespun to generate fibers for various applications. Both polymers are soluble in water and/or other solvents[43], biodegradable, biocompatible [6], physiologically

acceptable polymers and nontoxic for living organisms [44]. For PVP/ethanol solution, oxygen adjoins with hydrogen of ethanol [45] while for aqueous PEO solutions, PEO reacts with water to lead to a weak hydrogen bond [46]. Consequently, this bond increases solubility with the flexible polymer long chains. Because of the hydrophilic nature of such long structural chains, both polymers prevent protein adsorption [47] of bacterial responses [48]. As a whole, both PVP and PEO fibrous membranes are good capping agents, assisting charge transfer to inhibit bacteria efficiently[49].

It has been experimentally observed that PEO composite fibers with chitosan and embedded AgNPs exhibited good inhibition zone against Staphylococcus aurous(*S. aureus*) and Klebsiella pneumonia bacteria [50, 51]. On the other hand, well functionalized PVP/ZnO nanocomposites were fabricated via elctrospinning for use as an antimicrobial agent [52]. Apart from PEO and PVP fibers, Yalcinkaya et al. reported that the inhibition efficiency of Polyvinyl butyral(PVB)/CuO was over 90 % (much higher) since cupric ($Cu^{2+}$) ions can be distributed more homogenously in the fibrous membrane[53]. According to the comparison of antibacterial performance between Chitosan and PVP/ZnO composite fibers, Karpuraranjith et al, showed that PVP/ZnO inactivated gram positive and negative bacteria 17 and 6 % more than that for chitosan, respectively. Additionally, compared to Chitosan, Chitosan/PVP/ZnO nanocomposites increased the inhibition zone by 42 % more against *E. coli*. The reason behind this is that higher inhibition was possible because the effective capping agent, PVP fibers provided higher surface area where Zn NPs were evenly distributed to spoil biocidal activity [54]. Moreover, thermally, and chemically reduced Ag NPs embedded in PVP fiber-matrix promoted the uniform agglomeration of Ag NPs, assisting to interlink to a coordination bond with PVP (−N or −O) [55]. Higher molecular weight PVP tends to pattern uniform fibers with a smaller diameter distribution, eventually results in good interaction with NPs and exhibiting improved antimicrobial properties [3].

The microbial cell of bacterial strains attributes to very less longevity to ZnO, Ag and Cu NPs[1]. Throughout experiments, the inhibition efficiency of different heavy metal NPs has been investigated where the order of antibacterial activity against *E. coli* was demonstrated as following: CuO > ZnO = ZnO/ $TiO_2$ > $AgNO_3$ > $ZrO_2$ > $TiO_2$ > $SrO_2$ [56]. It is noticeable that PVB/CuO composites showed good results since the smallest diameter (244 nm) and high surface porosity (60.6 %) of CuO [56] could accelerate well emendation in the fiber's membrane. Being inspired

from these results, Ren et al. reported results on the antibacterial activities of CuNPs in that the CuNPs at higher concentrations could kill a wide range of bacterial pathogens [57, 58]. In fact, CuNPs have higher surface area, catalytic properties, good biocompatibility, stability and reactivity than AgNPs[59] which prompts to form $Cu^{2+}$ to dysfunction bacterial enzyme [3, 60]. More importantly, Cu is an engrossing antimicrobial agent because it is relatively cheap, easily mixed with polarized liquid and polymers[61].

The focus of the present work is to investigate the antibacterial functionalities of centrifugally spun PEO/Cu and PVP/Cu composite fibers against *E. coli and B. cereus* bacteria. CuNPs are very reactive and perilous to human body because of which nanofibrous membrane intermingled with CuNPs may potentially be a favorable for drug delivery and healing agent for human body. Typically, AgNPs are good antibacterial agent, however in this study, CuNPs were harnessed as an another alternative antibacterial agent, which are less expensive, highly active and more stable than AgNPs[59]. The present work focused on the capability, functionality, dissolution, and feasibility of centrifugally spun PEO/Cu and PVP/Cu composite fibers as a novel case to visualize the antibacterial activity. More importantly, the premise behind the study was to determine the optimum Cu concentration in fibers for the dysfunctionality of microbial attack. For this reason, two different polymers, PEO and PVP were selected since both are biocompatible, biodegradable and easily dissolved into very cost-effective solvents (water, ethanol). Additionally, the analysis based on the various experiments verified whether PEO or PVP fibers encapsulation of Cu NPs was feasible and if these fibers exhibit antibacterial inhibition at a various concentration of Cu.

## 2. Experimental

### 2.1 Materials

PEO and PVP with average Mw of 600,000 and 1,300, 000 were purchased from Sigma-Aldrich (St. Louis, MO, USA) and the solvent comprised of 100% pure deionized water (Distilled water) and ethanol. Cu nanoparticles with sizes of 40-50 nm were obtained from US Research Nanomaterials, Inc (Huston, TX, USA). All chemicals were used as received without further purification.

### 2.2 Preparation of Polymer/NPs composite fibers

PEO 8 % (w/w) and PVP 18 % (w/w) were dissolved in water and in ethanol, respectively. The solution was agitated by a Fisherband$^{TM}$ Analog Vortex mixer at 3200 rpm and then CuNPs of 15, 25 and 35 wt. % concentration, with respect to the polymer, were added to the solution. After the mixture was sonicated by Cole-Parmer 08895-12 Ultrasonic cleaner at 40 °C for 1 hour, the solution was then magnetically stirred by Thermo Scientific Cimarec+4x4 HP120, Cimarec Stirring Hotplates at 25 °C for 96 hours. The rotational speed of the stirring plate was 400 rpm. The proper homogeneous PEO/Cu and PVP/Cu solutions were then centrifugally spun using Cyclone L-1000M (Fiberio Technology Corporation) to produce the composite fibers. The as-prepared polymer solutions were injected into a spinneret equipped with 30-gauge half inch regular bevel needles. Adequate centrifugal forces were applied to the precursor solution to exceed the surface tension of the polymer jets and stretch out the fibers[30, 31, 41, 62, 63]. Centrifugal spinning was performed based at rotational speeds of 5000 rpm for PEO aqueous solution and 7500 rpm for PVP solution and at a relative humidity of 46%. The fibers were then collected in a well arranged eight uniform spacious vertical collectors while the collector was set at 12 cm from the spinneret. The PVP/Cu and PEO/Cu composite fibers were then kept in an Al foil and dried at 60 °C for 24 h in a vacuum oven.

**2.3 Characterization**

The morphology of PVP/Cu and PEO/Cu composite fibers was studied by scanning electron microscopy (FE-SEM; Sigma VP Carl Zeiss, Germany). Before conducting the SEM analysis, the samples were sputtered with a thin layer of gold coating using a Denton's Desk V deposition system to obtain high quality images. Then the average diameter of the samples was calculated from SEM images with 5 KX resolution by measuring 150 counts of various images using the image analysis software JMicroVision V.1.2.7 (University of Geneva, Geneva, Switzerland) and Origin Pro$^{@R}$ 2020 software.

EDS) analysis (EDAX, Mahwah, NJ, USA) was performed to evaluate the elemental composition of C, O, N and Cu nanoparticles in the fibers. The elemental composition of other different elements was scrutinized thoroughly for six of the samples where different areas were identified and peaks were obtained accordingly to those areas.

TGA analysis of PVP/Cu and PEO/Cu composite fibers was investigated by TA-Q series equipment, TGAQ500 (TA Instruments Inc.) under air environment. Samples of about 10 mg were kept in the instrument and heated from 25 to 700 °C under air flow at a heating rate of 5 °C/min.

XRD analysis was performed on the composite fibers to determine the crystal structure. A Bruker D2 powder (Bruker Germany) X-ray diffractometer was used with a Co source (Kα 1.789 Å), which was filtered using iron. The data were collected in 2θ from 10 to 80° with a count time of 5 sec and a step of 0.05° in 2θ.

Antibacterial activities against the gram-positive bacteria *B. cereus* and gram-negative bacteria *E. coli* were evaluated for both PVP/Cu and PEO/Cu composite fibers. The most standard antibacterial performance measurement method, Kirby Bauer disk diffusion method, was used where Agar plate was kept, and then the bacterial suspension was uniformly outspread onto the surface of agar plates by a sterile L-shape glass rod. The fibrous mats were then stored on the surface of agar plates to evaluate the inhibition zone of bacteria. During this test, the fibers were incubated at 37 °C for 72 hours.

In vitro release experiments were performed to determine the Cu release and sample stability. The copper-nanoparticles, PEO/Cu and PVP/Cu composite-fiber samples were suspended in 10 mL of deionized water (resistance 18 MΩ). The samples were placed on nutating mixer and equilibrated for 24 hours. Subsequent to equilibration, the samples were then removed and centrifuged at 3,000 RPM for 5 minutes and a 0.5 mL aliquot was extracted in triplicate. The extracted samples were saved and stored at 4 °C prior to analysis. The remaining samples were resuspended and placed back on the nutating mixer and equilibrated for additional 24 hours. This sampling and resuspending procedure was repeated every 48 hours for seven days The Cu concentration (released from the sample) was measured using Perkin Elmer 8300 Optima ICP-OES. The operating conditions of the ICP-OES were as follows: wavelength of 324.7 nm, nebulizer flow of 0.65 L/ min, plasma flow of 20 L/min, an auxiliary flow of 0.2 L/min, and RF power of 1500 W while an integration time of 20s was used per replicate. The data analysis was performed in triplicate.

## 3. Results and Discussions

### 3.1 Morphology and structure of fibers

The finest structure and morphology of the centrifugally spun Cu/PEO and Cu/PVP composite fibers were obtained from the selective spinneret rotational speed, polymer concentration, viscosity, relative humidity, and the spinneret-to-collector distance. The effective combination of these parameters results in bead-free and uniform nanofibrous matrix. During centrifugal spinning, PEO aqueous solution of 8 wt.% concentration[42] produces bead-free fibers. In the case of PEO solution, the viscosity at 8 wt.% concentration[42] was very low to produce good fibrous mats whereas a higher viscosity than this one yielded beaded and torn fibers[64]. Here the experiments were performed at 46-48% the relative humidity since aqueous solution didn't get it evaporated beyond upper of this humidity. Mostly in that case, enough vapor could not suck out existent water from the solution. During centrifugal spinning of PEO/Cu composite fibers, the spinneret rotational speed was set between 5500 and 8000 rpm at a favorable humidity. However, the centrifugal spinning of PEO/Cu solutions at rotational speeds lower than 4500 rpm barely produced morphologically uniform fibers due to the high surface tension of the polymer droplets[65]. Conversely, at rotational speeds above 9000 rpm, the centrifugal forces exceeded the solution's surface tension and resulted in fiber breakage[33, 66]. As a result, at shorter spinning time, more jets were ejected onto the collector swiftly and negatively affected the deposition of fibers on the collector. Finally, PEO/Cu solutions with 15, 25 and 35 wt. % CuNPs were centrifugally spun to obtain uniform and layered fibers. Similarly, the PVP/ethanol solution was more favorable to be spun at 21 wt. % concentration. Solutions having concentrations lower than 21 wt. % were difficult to get fibers as the viscosity was lower while concentrations more than 28 wt% were cumbersome to spin. For the spinneret rotational speed, 7500 rpm was a good value to get fine fibers at a favorable humidity. Experimentally, PVP/Cu solutions were centrifugally spun at 7500 rpm for three different Cu concentrations of 15 %, 25 % and 35 wt. % which resulted in fibers with different morphologies. Figure 1 shows the SEM images of PEO/Cu composite fibers. The fibers (Figure 1 (A, C, E)) were uniform, slender, and well-arranged. The histograms in Figure 1 (B, D, F) clarify that the diameter of PEO/Cu composite fibers decreased with increasing the CuNPs loading in the PEO-fiber matrix which was in agreement with previous experimental results[42]. The SEM image in Figure 1C showed bundled PEO/Cu composite fibers. Several factors can lead to the formation of bundled fibers such as the distance between the collector and spinneret, solvent evaporation rate, vapor pressure of the solvent and van der Waals attraction between fibers[67]. A short distance between the spinneret and collector (12 cm in the present

setup which is the maximum distance) results in the formation of wet fibers that can easily bundle together on the collector. In fact, a slow evaporation rate of the solvent (e.g., water or DMF) will lead to the formation of wet fibers and once they are deposited on the collector, the fibers start to bundle. Using a solvent with high vapor pressure such as ethanol, acetone and chloroform can increase the evaporation rate and hence reduce the adhesion between the fibers. Therefore, increasing the spinning time, collector-to-spinneret distance, temperature, and time of evaporation of the solvent can reduce the adhesion between fibers and ultimately prevent the formation of bundled fibers. Future work in our group will focus on the effect of solvent-type and binary solvent mixtures on the fiber formation and morphology of centrifugally spun composite fibers.

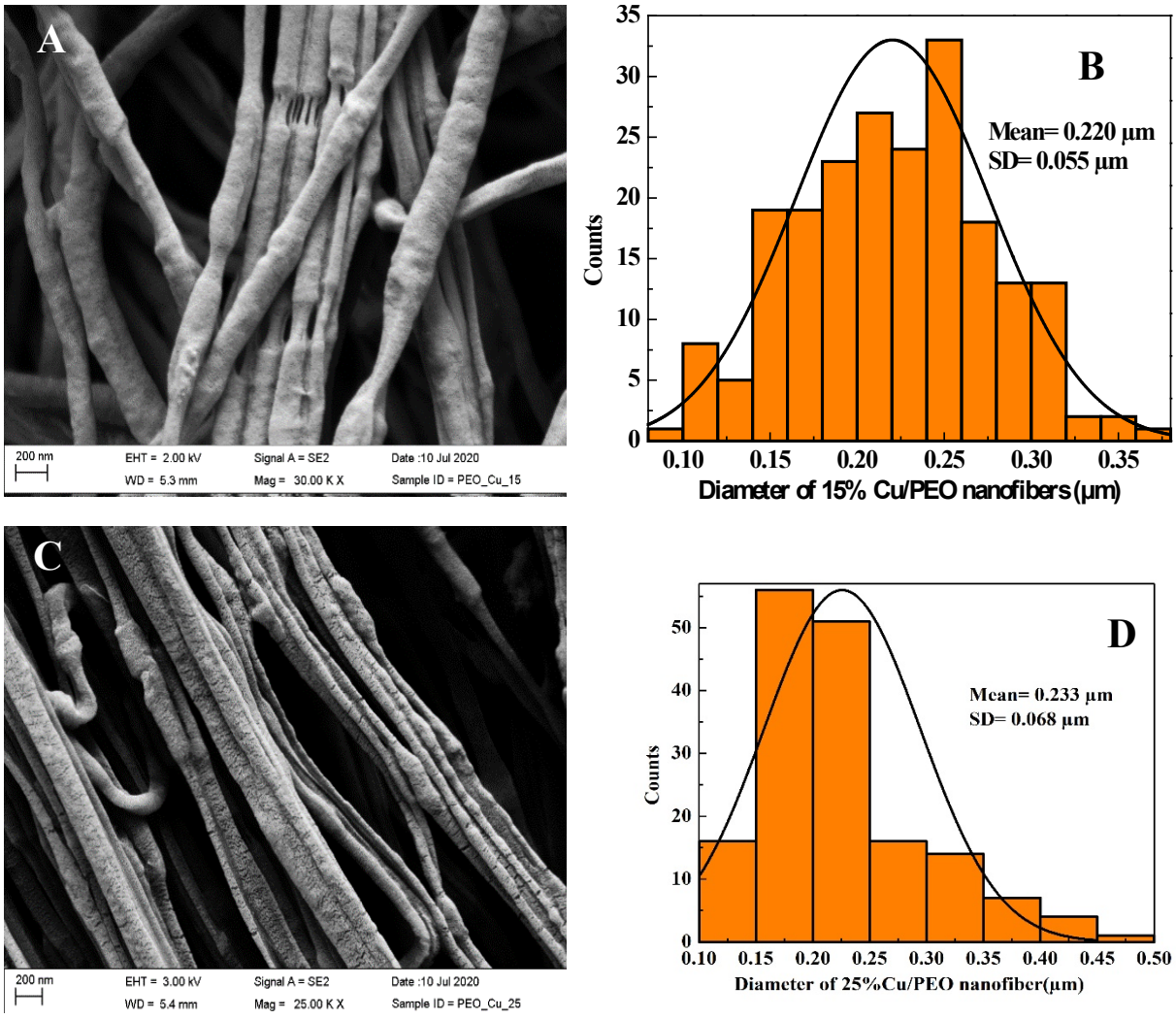

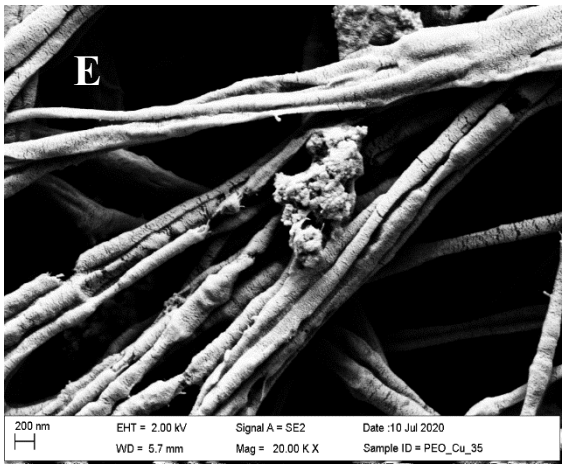


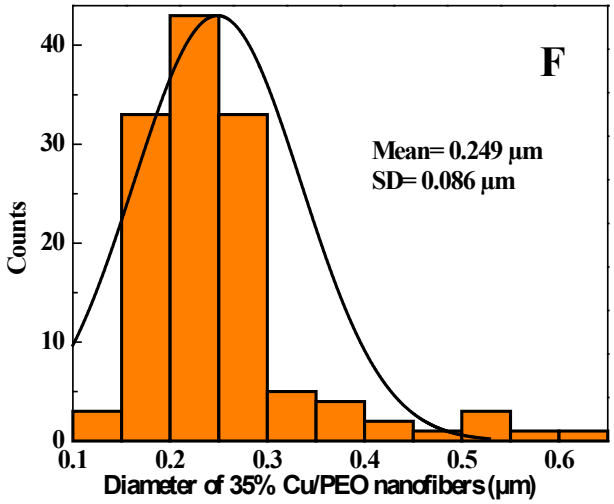


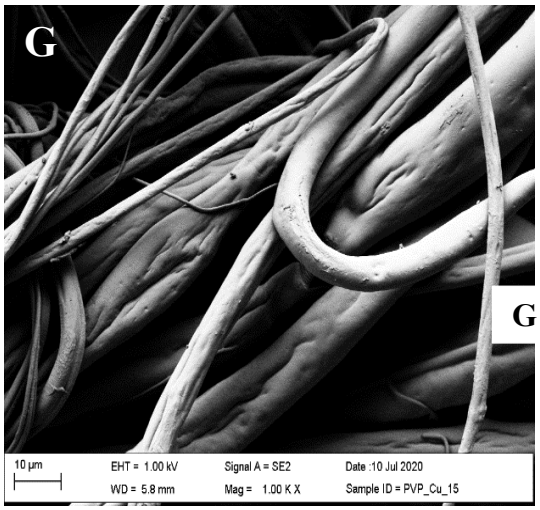


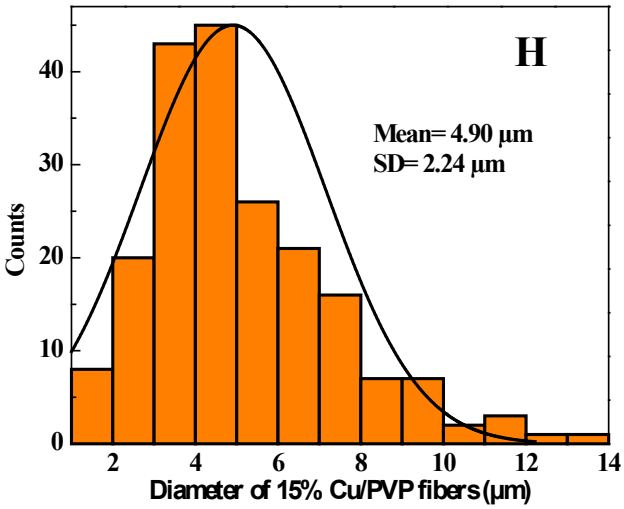


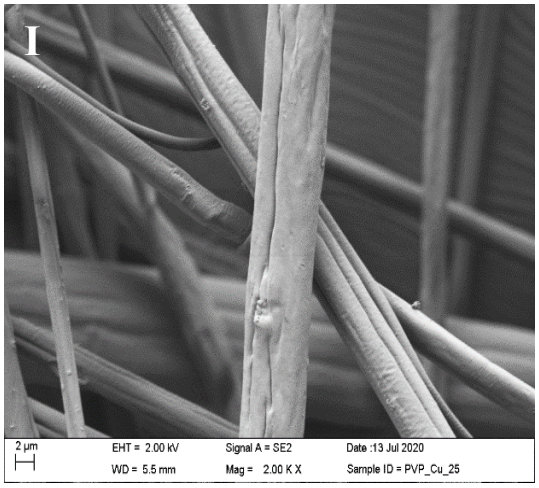


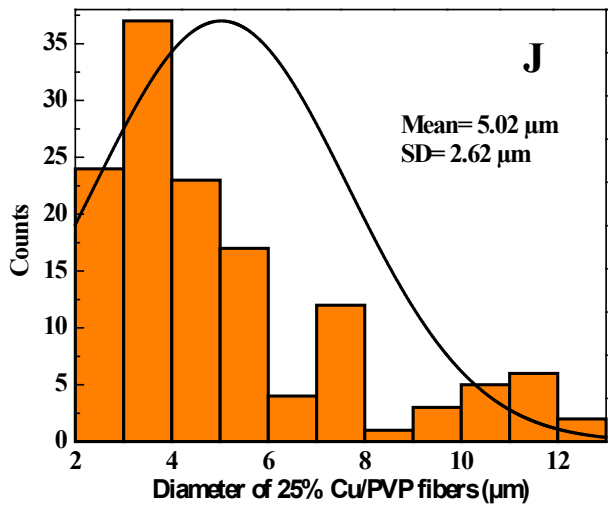

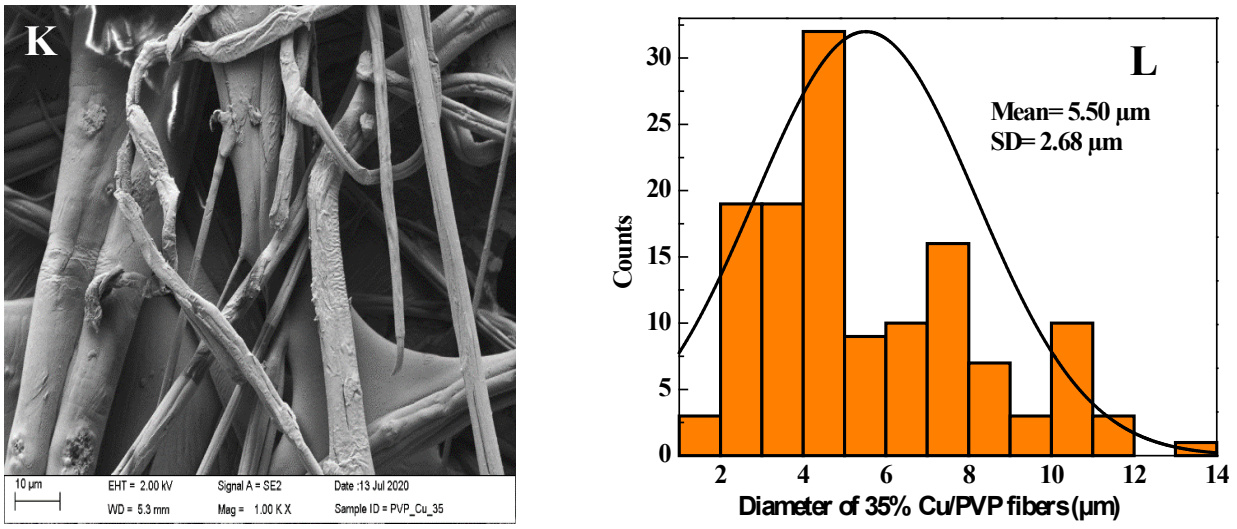


Figure 1: SEM images of the PEO/Cu and PVP/Cu composite nanofibers with 15, 25, and 35 wt. % Cu NPs concentrations in the precursor solution ([A, C, E], [G, I, K]) respectively. The average fiber diameter distribution (histograms) ([B, D, F], [H, J, L]).

Furthermore, the SEM image in Figure 1 A showed that the fibers were lightly deformed from a cylindrical shape. The deformation may be due to the higher spinning speed with a shorter run time. In fact, polymer droplets might not have had enough time to be swelled and stretched properly at room temperature, which resulted in loss in the capability to softening into cylindrical shape properly[68]. Naturally nano/micro fibrous mats can be broken up due to lower vapor pressure of solvent where coalescing fibrous layers get lost due to easier relaxation of polymer chains into non-stretched conformation at slow drying process[69]. Additionally, the jet can break up due to viscous force, imbalance of centrifugal forces and surface tension. Furthermore, centrifugal and air drag forces can break up fibers from solutions with low viscosity where stretching was impeded and torn away [70, 71]. In addition, in centrifugally spinning the fibers are more loosely packed than in electrospinning because of the absence of the electric force field [72]. Considering all reasoning for fiber deformation/ breakage it may be clear that at 15 wt. % PEO/Cu precursor solution, the viscosity was lower, which led to the breaking of fibers in some parts, which was noticed.

Moreover, the SEM images shown in Figure 1 (A, C, E, G, I and K) confirmed that the increase of Cu concentration in the PEO and PVP solutions resulted in bead-free PEO/Cu and PVP/Cu

composite fibers. Basically, the metal nanoparticles (Cu NPs) assisted in reducing the crystallinity of the polymer as well as shortened the size of crystallites of spherulites[73]. Eventually, the Cu NPs can disrupt the crystal portion and increase the amorphous region in the polymer matrix to enhance smoother morphology. PEO/Cu nanofiber's diameter ranged from 220 to 249 nm while the PVP/Cu nanofiber's diameter was within 4900 to 5500 nm (Figure1, A, C, E, G, I, and K). Higher Cu concentrations in the polymer solution resulted in fibers with higher average fiber diameters as observed in the diametrical statistical analysis (histograms). The Cu NPs were mainly embedded into the core/shell of fibers as well as attached to the outer surface of the nano fibrous membrane. If nanoparticles were attached to the outer surface, then the NPs sometimes tended to agglomerate to form clusters on the fiber surface. From the morphological surface analysis, PEO/Cu fibers (Figure 1, A, C, E) were flatter and thinner than PVP/Cu fibers (Figure 1, G, I, K). As a semi crystalline polymer, PEO with water as the solvent gets enough advantages to disperse more and keeps its crystallinity while the amorphous phase of PVP fibers makes its nanofibrous membrane disordered and bended in various portion (Fig I, K)

### 3.2 Elemental Mapping Analysis

EDS analysis was performed to investigate the elemental composition of the PEO/Cu and PVP/Cu composite fibers. Figure 2A shows the EDS mappings of 15 wt. % Cu/PVP composite fibers. Based on a short sample area, the presence of C, N, O, Cu are detected as 79, 4, 8 and 9 wt.% respectively, according to their composition percentages. Similarly, Figure 2B indicates the elemental composition of 15 wt, % of Cu/PEO composite fibers where C, O and Cu are present in 73, 14 and 14 wt. % percentages, respectively.

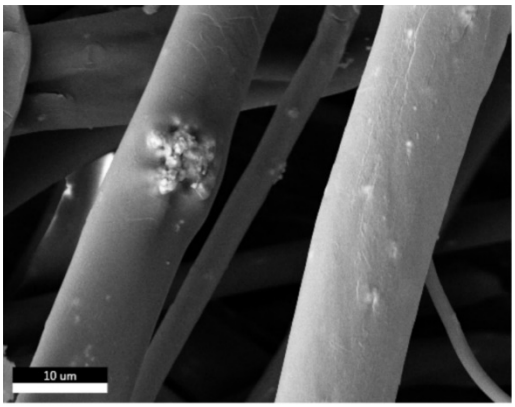


SEM Image

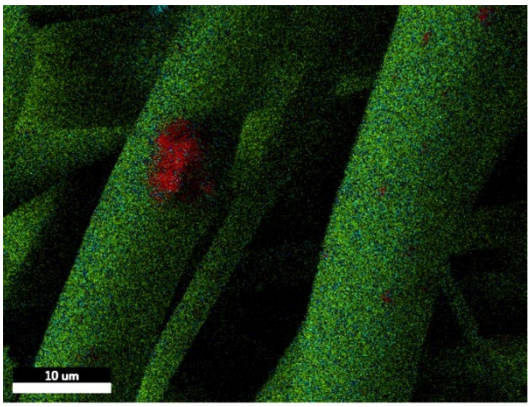


Mapping Sample Area

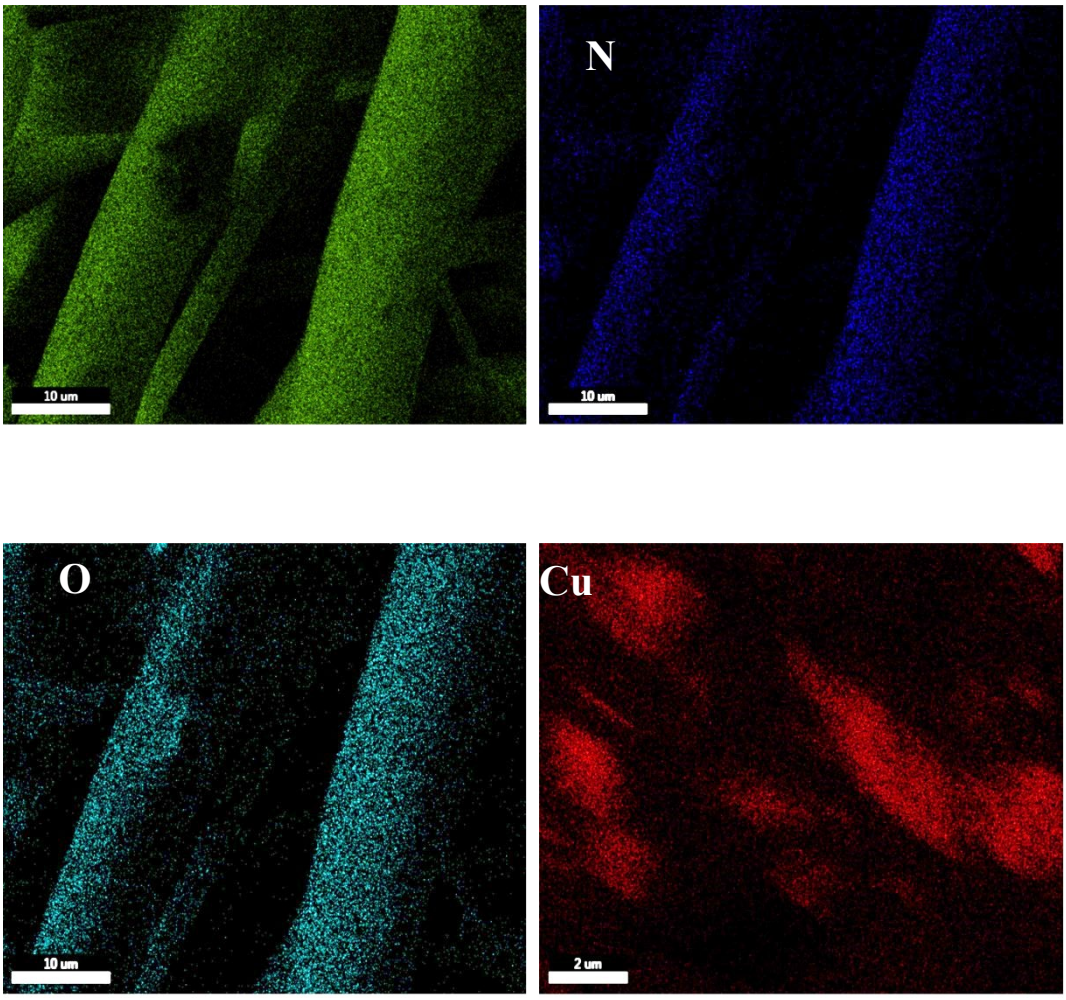


Figure 2A: Elemental composition of PVP/Cu Nano-fibrous membrane

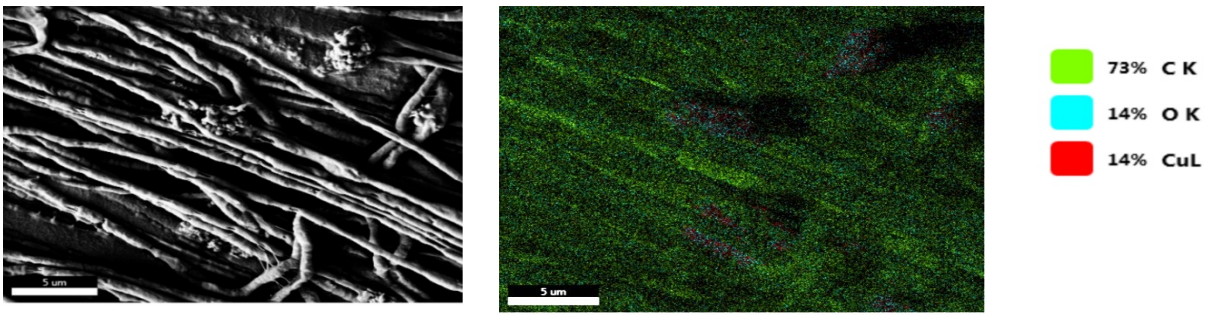


SEM Sample area

Mapping Sample Area

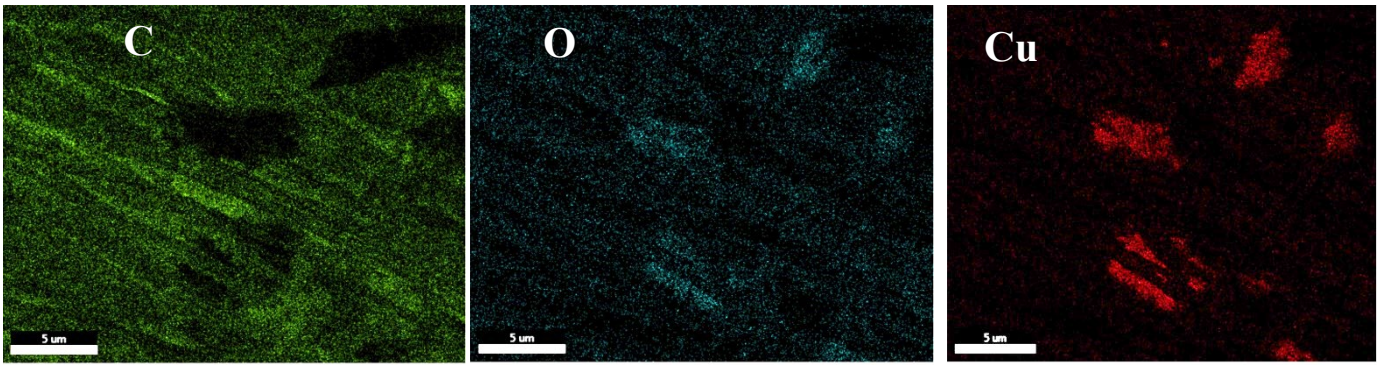


Figure 2B: Elemental composition of PEO/Cu Nano-fibrous membrane

The EDS mappings in Figures 2A and 2B clearly show the presence of Cu C, O and N elements embedded in the PVP and PEO fibers

**3.3 Thermogravimetric Analysis:**

Thermal degradation of the PEO/Cu and PVP/Cu composite fibers was investigated by TGA under air environment. PEO/Cu and PVP/Cu composite fibers of 15, 25 and 35 wt.% Cu concentrations (Figure 3) represent similar congruity in the TGA results with few changes caused by the addition of Cu NPs variously. At a temperature between 25 and 700 $^{\circ}$C; the weight loss of fibers was vividly apparent because of the thermal ignition. The pristine PEO fibers were almost volatilized completely at about 550 $^{\circ}$C, with a low amount of char being noticed (Figure 3A) while the pristine PVP fibers were vaporized finely at 600 $^{\circ}$C.

At a temperature range between 25 and 200 $^{\circ}$C, 3 % weight loss of PEO fibers was caused by water evaporation to form anhydride while in the case of PVP fibers, ethanol was quickly vaporized within this temperature range since PVP has more vapor pressure than water (Figure. 3A). Basically, due to solvent disappearance, the polymer matrix suffers from volume shrinkage and its morphology gets vertical where nanofillers, CuNPs are not affected. Therefore, the peak at 80 $^{o}$C (Figure 3C) represents the removal of ethanol physically absorbed by the PVP-fiber surface[74]. In the second temperature region from 200 to 400 $^{\circ}$C, the weight loss of the PEO/Cu nanocomposite fibers is highly noticeable where the internal polymeric matrix loses weight during the thermal degradation. In this section, PEO loses its branching and cross-linking in order to initiate release chain scission[75]. Overall, the small cross-sectional area of fibers prepared from aqueous PEO solutions contributes to the semi-crystalline phase which also turns to fully degraded as losing polymeric chains[76]. On the other hand, for PVP/Cu nanocomposite, the polymer fibers

get more thermally decomposed from 250 to 450 ºC. In fact, PVP is an amorphous polymer whose disordered polymer chain is more thermally stable. As a result, PVP decomposes its chemical structure after a significant temperature change as indicated in Figure 3C. Therefore, PVP fibers under oxidation at 300 to 400 ºC yields carbon dioxide and pyrrolidone which is apparent at the TGA peaks (350 ºC) terminating the strained sections of the polymer chain[74]. At about 600-700 ˚C, the residual weight fraction was caused by the experimental errors which was exactly concurrent with the Cu NPs loading in the PVP-fiber matrix (Fig 3A, 3B). Similar to the TGA curve analysis, the derivative of thermal degradation (DTG) indicates the correspondent dissociation of weight percentage loss with the temperature. At low temperature (up to 200 ˚C), the rate of change of weight loss is constant indicating the zero-derivative portion in PEO fibers (Fig 3B), water just vaporized at a constant phase change. Thus, in this section, the polymer degradation is unnoticeable, probably reflecting negligible amounts of water still captured within the fibers. Reversely, for PVP fibers, more volatile ethanol gets easily dried within 120 ˚C where the thermal degradation is quite fast (Fig 3D). Most importantly, the main degradation process occurs from about 225 to 450 ˚C for PEO fibers while for PVP fibers, it is from 300 to 450 ºC. In this temperature range, the CuNPs are essentially shifting the degradation temperature slightly towards higher temperatures. It is observed in Fig 3(B and D) that the weight loss for all samples remains unchanged between 450 and 700 ˚C, indicating that the decomposition of the polymer-fiber matrix is completed. The residual mass at 700 ˚C is negligible for the pristine PEO and PVP fibers and consistent, within the experimental errors, with the content of CuNPs (near about 0 wt. %) in the PEO and PVP fiber-matrices. The derivative of the residual mass as a function of temperature (Figs 3B and 3D) represents two negative degradation peaks in the various wt.% of PEO and PVP fibers. These peaks are located at a temperature where the weight loss is maximum and eventually suggest two competing degradation mechanisms[77]. Basically, the incorporation of CuNPs in the PEO and PVP fibers narrows these peaks and shift them slightly to higher temperatures, signifying that CuNPs and polymer fibers are bonded adhesively, and dissociation temperature of both fibers are higher. At about 35 wt.% of CuNPs, there are essentially a single major degradation peak at about 400˚C and some minor broad peaks at lower temperatures.

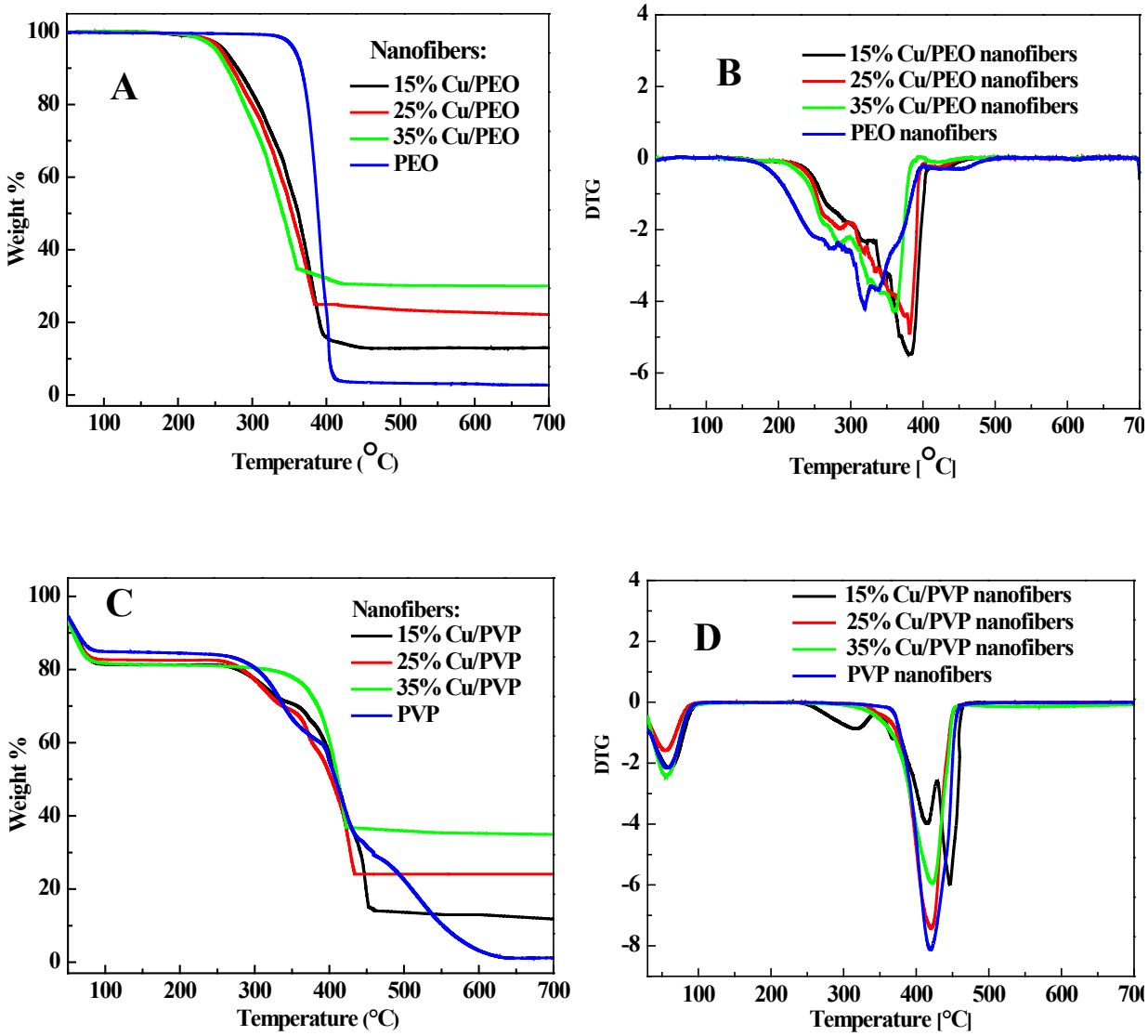


Figure 3: Thermal Gravimetric Analysis of (A) PEO/Cu & (C) PVP/Cu nanofiber. Gravimetric Thermal Derivative Analysis of (B) PEO/Cu & (D) PVP/Cu.

### 3.4 XRD Results

Figure 4 A shows the collected diffraction patterns for the PEO fibers which are consistent with those reported by Takahasi and Tadokoro on PEO powder [78]. The Le Bail fitting and determined lattice parameters are illustrated in Table 1. The fitting has a $\chi^2$ of 1.70 which indicates a good agreement between the data of the crystal structure. The diffraction pattern for the PEO/Cu composite fibers (Figure 4 B) confirms the presence of three phases (the two large diffraction PEO

peaks at 22.08 and 26.94 in 2θ), Cu metal, and CuO. The CuO diffraction peaks observed in the sample represent the 110, 002/-111, 111/200, -202, and 113 planes, which were located at 37.710, 41.23, 41.38, 45.03, 45.31, and 73.64, in 2θ, respectively [79]. The Cu metal phase showed the 111 and 200 diffraction peaks which were located at 50.28 and 59.213 in 2θ, respectively [80]. The Le Bail fitting of the PEO-Cu composite fibers had a very good $\chi^2$ value of 1.72 indicating a good agreement between the experimental data and fitting.

The diffraction pattern of PVP fibers is shown in Figure 4 A which consisted of two diffuse-weak peaks located at 13.30 and 25.35 in 2θ. The XRD results of PVP fibers are consistent with those reported in the literature on PVP powder [81]. The diffraction pattern was not fitted due to the amorphous phase present in the sample. The diffraction patterns of the PVP/Cu composite fibers are shown in Figure 4 B. The diffraction pattern of the sample consisted of three phases: two PVP diffraction peaks at 13.30 and 25.35 in 2θ, CuO and Cu metal. The CuO phase showed the 002, -111, 1211. The Cu 111 and 220 diffraction planes were observed in the Cu phase at 50.280 and 59.213 in 2θ, respectively. The Le Bail fitting results of the PVP/Cu composite fibers shown in Table 1 had a $\chi^2$ of 1.35, again indicating an excellent agreement between the proposed phases and the experimental data.

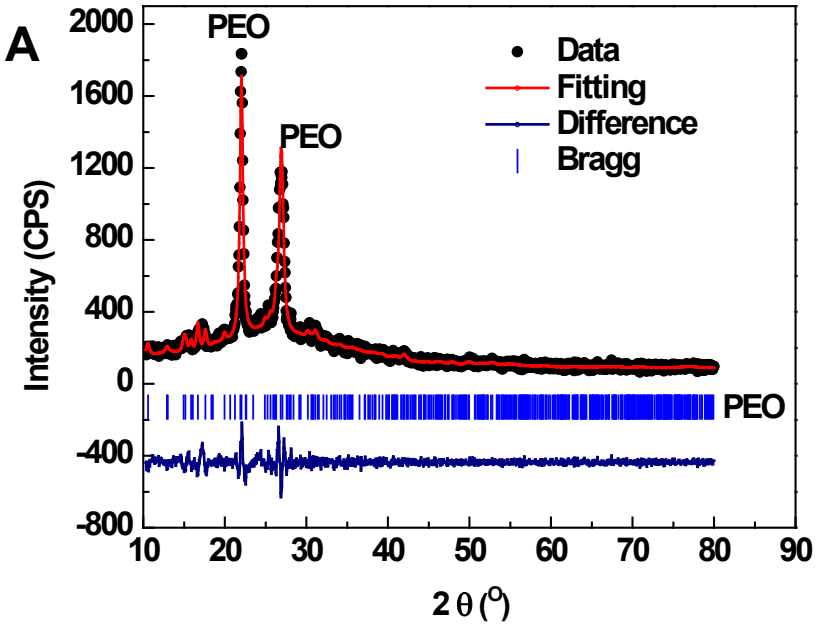

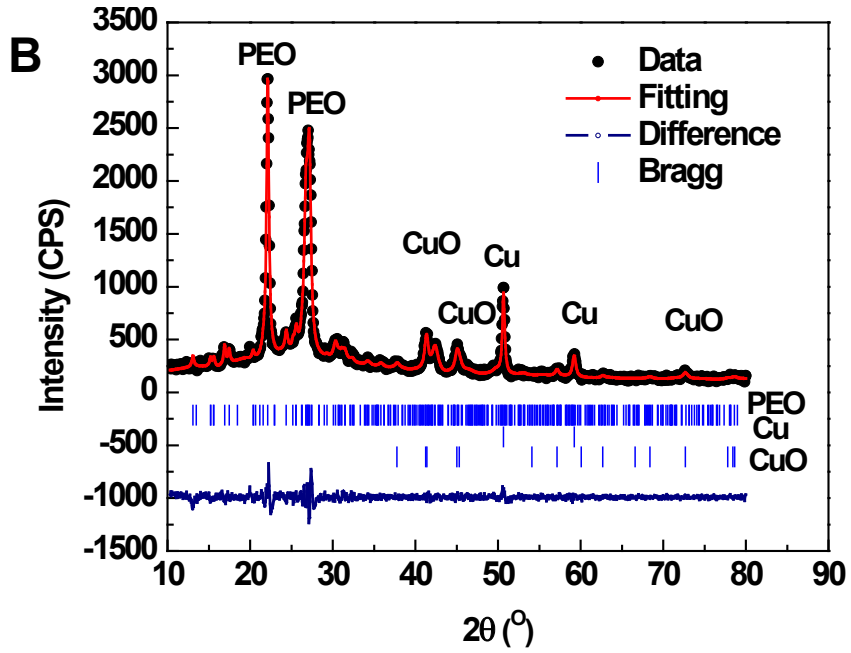


**Figure 4: A.** Le Bail fitting of the diffraction pattern collected for the PEO fibers. **B.** Diffraction pattern collected for the PEO/Cu composite fibers.

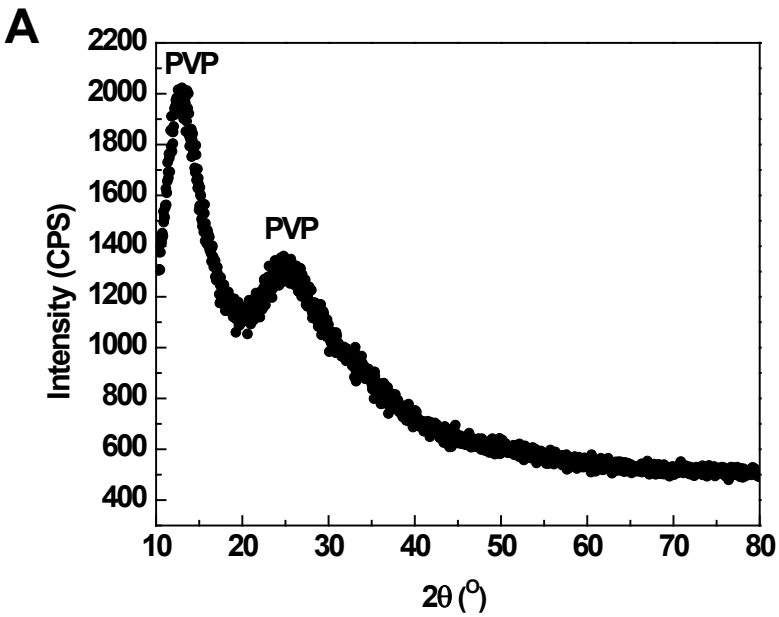

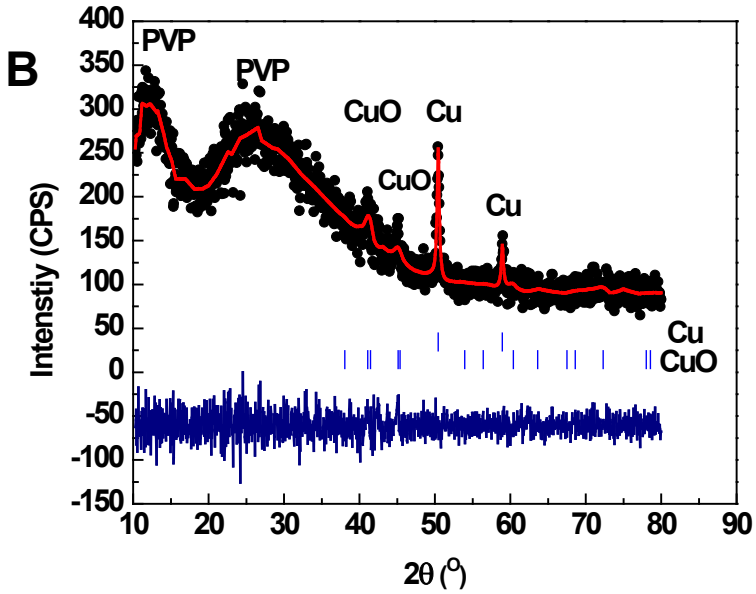


**Figure 4. B.** Collected diffraction pattern of PVP fibers. **B.** Le Bail fitting of the PVP fibers with Cu NPs embedded in the fibers.

**Table 1:** Le Bail Fitting parameters for the PEO, PEO/CuNPs and PVP/Cu NPs

| Sample | Phase | Space Group | a(Å) | b(Å) | c(Å) | α(°) | β(°) | γ(°) | $\chi^2$ |
|---|---|---|---|---|---|---|---|---|---|
| PEO | PEO | $P2_1/c$ | 8.00(8) | 13.20(3) | 19.53(1) | 90.00 | 123.89 | 90.00 | 1.70 |
| PEO-Cu | PEO | $P2_1/c$ | 8.00(8) | 13.20(3) | 19.53(1) | 90.00 | 123.89 | 90.00 | 1.75 |
| | CuO | C2/c | 4.691(5) | 3.249(2) | 5.132(3) | 90.00 | 99.23 | 90.00 | |
| | Cu | $FM\bar{3}M$ | 3.610(1) | 3.610(1) | 3.610(1) | 90.00 | 90.00 | 90.00 | |
| PVP-Cu | CuO | C2/c | 4.738(6) | 3.249(3) | 5.181(4) | 90.00 | 99.23 | 90.00 | 1.35 |
| | Cu | $FM\bar{3}M$ | 3.638(9) | 3.638(9) | 3.638(9) | 90.00 | 90.00 | 90.00 | |

### 3.5 Antibacterial Performance

As antibacterial agents, PEO/Cu and PVP/Cu nanofibrous membranes of different concentrations (15, 25 and 35 wt. %) were tested for the antibacterial performance against the gram-negative *E. coli* and gram-positive *B. cereus* bacteria. In the disk diffusion method, fibers were kept on a cleaned agar plate contained with both bacteria for 72 hours. Figure 5 (A-C) shows the assessment of the growth of inhibition zone formation as an antimicrobial activity against *E. coli* by PEO/Cu (15, 25 and 35 wt. %) while Figure 5 (D-F) indicates activity by PVP/Cu (15, 25 & 35 wt. %) composite nanofibrous membranes.

Inhibition zone formation against *E. coli* bacteria

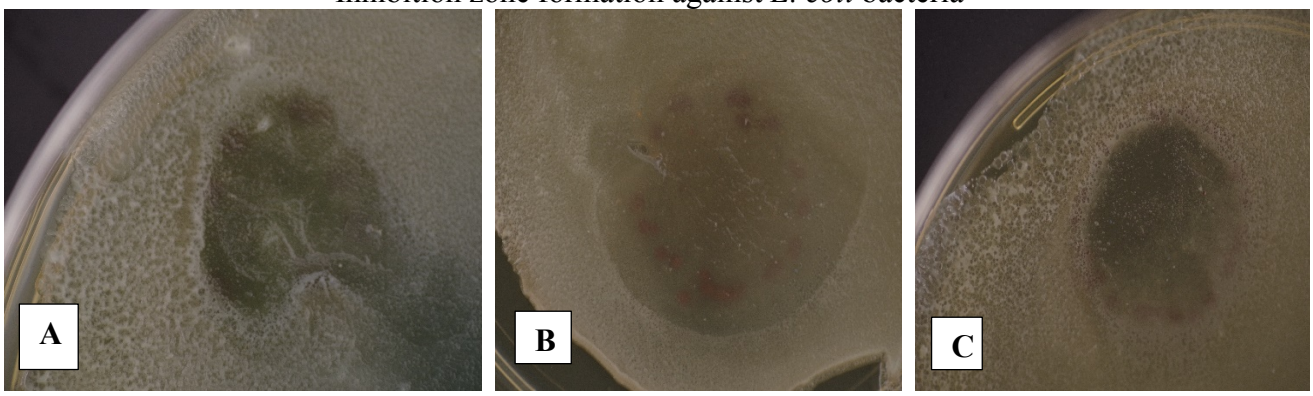


Inhibition capacity 53.14%
15% Cu/PEO nanofiber

Inhibition capacity 71.2%
25% Cu/PEO nanofiber

Inhibition capacity 93%
35% Cu/PEO nanofiber

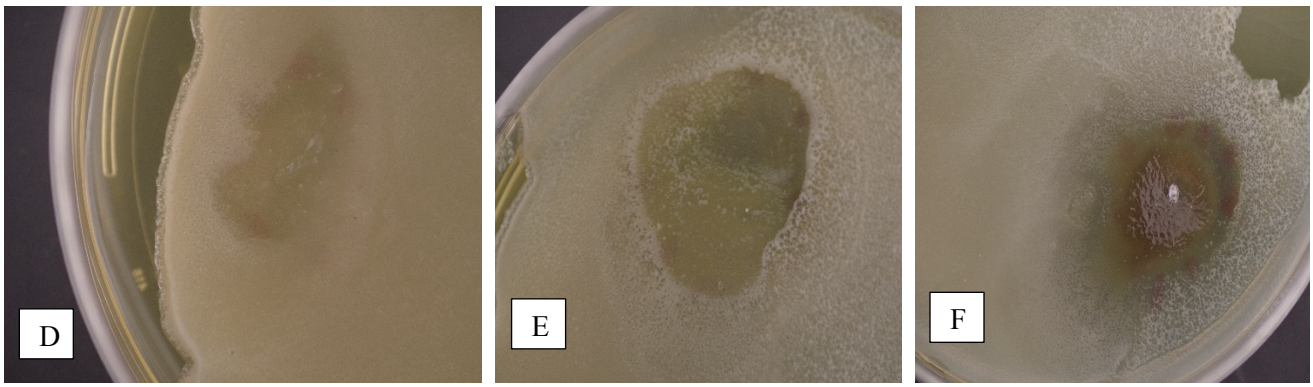


Inhibition capacity 47%
15% Cu/PVP nanofiber

Inhibition capacity 85%
25% Cu/PVP nanofiber

Inhibition capacity 90%
35% Cu/PVP nanofiber

On the other hand, the growth of inhibition zone against *B. cereus* bacteria by PEO/Cu and PVP/Cu composite fibers are shown in Figure5 (G-I) and J-L), respectively.

Inhibition zone formation against *B. cereus* bacteria

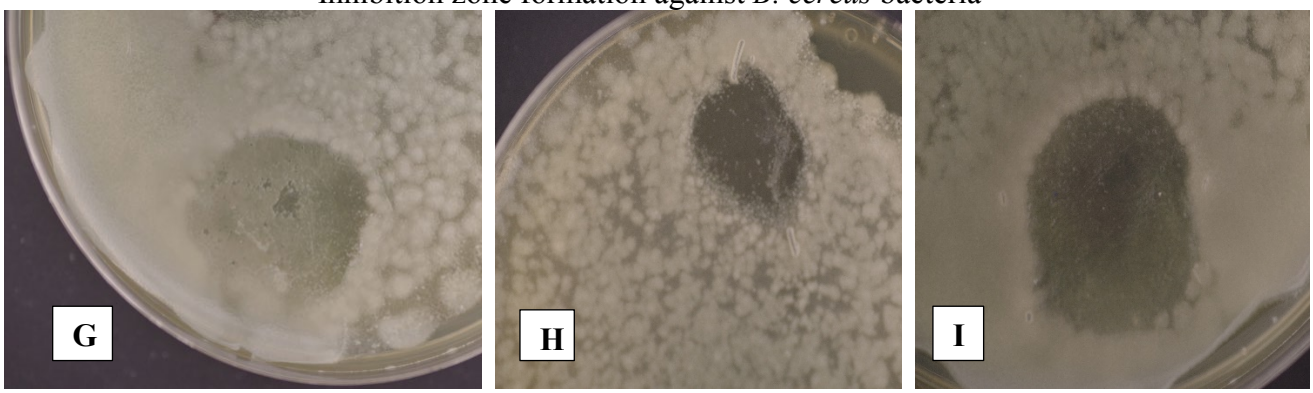


Inhibition capacity 18%
15% Cu/PEO nanofiber

Inhibition capacity 89%
25% Cu/PEO nanofiber

Inhibition capacity 100%
35% Cu/PEO nanofiber

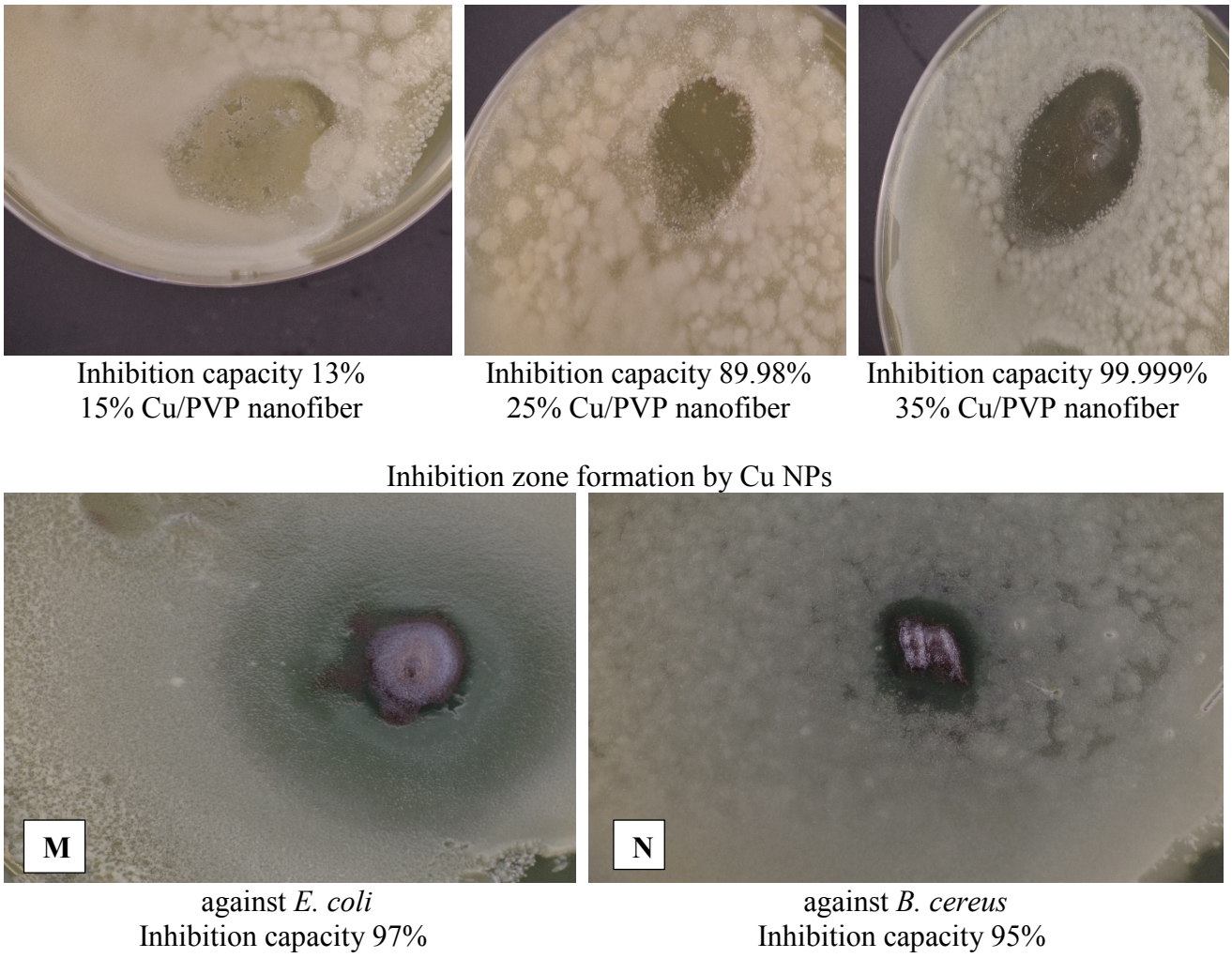


Figure 5: Inhibition zone visible on the Agar Plate in PEO/Cu fibers of 15, 25 and 35 wt % nanoparticles.

Finally, the antimicrobial activity of CuNPs was shown and its clear inhibition growth zones were indicated against in *E. coli* (Figure 5M) and *B. cereus* (Figure 5 N). From the experimental data, it was observed that the inhibition zone growth against gram negative, *E. coli bacteria* in PEO/Cu composite fibers was 53.14, 71.2 and 93 % for Cu concentration of 15, 25 and 35 wt.%, respectively in 72 hours (Figure 5, A, B, C) where the average inhibition diameter was 1.64 out of 2.258 cm. Reversely, PVP/Cu fibers showed inhibition zone efficiency of 47, 85 and 90 for 15, 25 and 35 wt. % Cu concentration presented in fibers, respectively. As a capping agent, Cu NPs can be embedded effectively in PVP fibers at higher concentrations of Cu nanoparticles. For this

reason, the average inhibition diameter was 1.671 out of 2.258 cm in PVP/Cu nanofibrous membrane where bacteria grew less than PEO/Cu membrane. On the other hand, in gram positive bacteria, *B. cereus* bacteria; the growth percentage of the inhibition zone capacity (Figure 5, G, H, I) was 18, 89 and 100 % in case of PEO/Cu fibers while for PVP/Cu fibers, Figure 5 (J, K, L), the inhibition zone capacity was 13, 89.98 and 99.99 %. Moreover, the Cu NPs were proved as a good antibacterial agent since in CuNPs, *E. coli* and *B. cereus* bacteria were inhibited at 97 and 95 % (Figure 5, M, N) respectively.

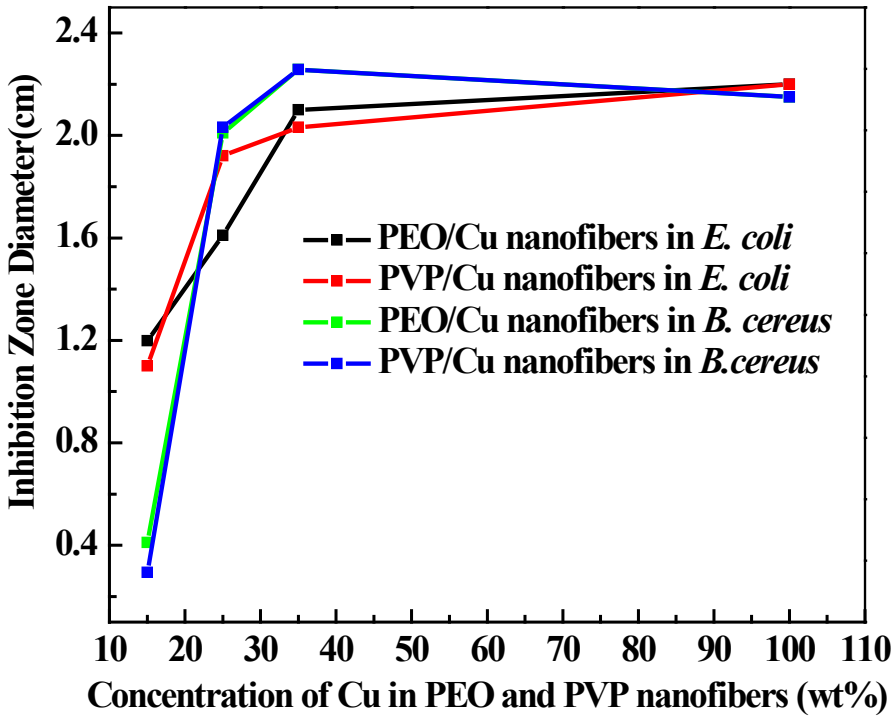


**Figure 6:** Relationship between Cu concentration in PEO/PVP nanofiber and corresponding inhibition zone diameter (the nanofiber's sample size was 2.258cm).

From Figure 6, it is apparent that the inhibition capacity of PEO/Cu was higher than PVP/Cu nanofibrous membranes. Again, the inhibition zone formation on *E. coli* was more than *for B. cereus* as was observed in Figure 5 because the cell structural of gram *E. coli* is composed of thinner cell wall thickness of peptidoglycan while *B. cereus* is thicker cell wall which is very hard to permeate[82]. Within 72 hours, *E. coli* was nearly fully inhibited by the membrane while *B. cereus* was less inhibited than *E. coli*. Therefore, the PEO/Cu nanofibrous membranes were more

effective to impede gram negative bacterial strain where the strain can easily be paralyzed by fibers. However, the *B. cereus* bacterial strain was more capable to propagate alongside the nanofibrous membrane. Therefore, the inhibition zone efficiency in *B. cereus* was a bit lower than *E. coli*.

Table 2: Inhibition Zone diameter for the Antibacterial Activity of PEO/Ag fibers

| Fibers in bacteria | Average diameter of inhibition zone(cm) | Standard Deviation (mm) |
|---|---|---|
| PEO/Cu in *E.coli* | 1.64 out of 2.258 | 0.45 |
| PEO/Cu in *B. cereus* | 1.6841 out of 2.258 | 0.51 |
| PEO/Cu in *E. coli* | 1.558 out of 2.258 | 1.005 |
| PEO/Cu in *B. cereus* | 1.528 out of 2.258 | 1.0749 |

For the measurements of the inhibition zone diameter was taken after three days of inhibition of bacteria I the presence of composite fibers. The average inhibited zone diameter of PEO/Cu nanofibers on *E. coli* was then found to be 1.64 cm out of the sample diameter (2.258 cm) and in the case of *B. cereus* bacteria, the diameter was 1.6841 cm. Reversely, PVP/Cu fibrous membrane inhibition capacity (as an average diameter) was found to be 1.558 and 1.528 cm in *E. coli* and *B. cereus* bacteria, respectively. This antimicrobial function of nanofibrous membranes was due to the higher surface area to volume ratio of fibers dispersed into the homogeneous Cu nanoparticles. Since Cu nanoparticles have antibacterial activity, with fibers, their function was visualized as indicated in Figure 5. Basically, Cu NPs were ionized as $Cu^{2+}$ which played a role to captive the negative ion of cell structure and inactivate the DNA replication stability. As a result, both gram positive and negative bacteria were sterilized quickly. From the values illustrated in Table 1, it is evident that 35 wt. % Cu NPs embedded in nanofibrous PEO and PVP membranes were a finer agent than other metallic oxides to inhibit bacteria.

### 3.6 Cu NPs release and stability results

Cu NPs stability tests were performed to investigate the $Cu^{2+}$ ion release from pure Cu NPs, Cu/PEO, and Cu/PVP composite fibers. Dissolution of $Cu^{2+}$ ions from the different samples was investigated over one week with ultra-pure water. The results for the Cu-nanoparticle sample (Figure 7A) showed that the $Cu^{2+}$ concentration initially increased at 24 hours, decreased after 48 hours, and then increased continually up to 168 h. The observed decrease in the $Cu^{2+}$ concentration might be due to the oxidation of the Cu-nanoparticle surface, which would generate binding sites on the nanoparticles. These binding sites may then have led to an adsorption of free $Cu^{2+}$ ions from the solution onto the nanoparticle surface. The dissolution processes should overcome the surface complexation over time, hence resulting in an increased release of $Cu^{2+}$. It can be observed in Figure 7 B that the 15 wt. % PVP/Cu composite-fiber -sample showed an increase in $Cu^{2}$+ concentration with increasing time, which reached a maximum value at 168 h. However, the 15 wt. % PEO/Cu composite fibers showed a similar trend of increasing $Cu^{2+}$ concentration with increasing time (Figure 7 C). As can be seen in Figures 7 D and 7 E, both the 25 wt. % PVP/Cu and PEO/Cu composite-fiber samples showed a similar behavior of increasing concentration with increasing time. However, the 25 wt. % samples reached maximum of $Cu^{2+}$ concentration in solution faster than the 15 wt.% samples, with 72 hours of reaction. The 35 wt. % PVP/Cu composite-fiber sample showed a different behavior compared to other samples. Within the first 24 hours of the study, the maximum concentration of $Cu^{2+}$ was released while the concentration remained constant up to the 168 h, as can be seen in Figure 7F. The 35 wt. % PEO/Cu samples showed a similar behavior to that of the 25 wt. % PEO/Cu composite fibers where an increasing in $Cu^{2+}$ concentration was observed at increasing time while equilibrium was reached within the first 72 hours and remained constant thereafter. It should also be noted that the PEO/Cu composite-fiber samples consistently had a lower dissolution of Cu NPS as can be seen by the low concentration of $Cu^{2+}$ in solution, which maximized at 0.25 ppm. On the other hand, the Cu-nanoparticle sample reached a maximum consideration of $Cu^{2+}$ at approximately 3 ppm while the 15%, 25% and 35% PVP/Cu composite-fiber samples showed a maximum of $Cu^{2+}$ concentration at approximately 3.0, 2.25, and 1.8 ppm, respectively. The difference in behavior between the PVP/Cu, PEO/Cu, and Cu-NPS samples can be explained by the attachment of surface groups to the Cu nanoparticles. The Cu-nanoparticle samples do not have a surfactant covering the nanoparticles, which makes them readily available for dissolution. However, the PVP and PEO in

the PVP/Cu and PEO/Cu composite fibers act as surfactants on the nanoparticle surface and aide in slowing or reducing the dissolution of $Cu^{2+}$ ions. In fact, PVP has a terminal ketone group in its backbone, which does not bind to metal ions or particles very easily. On the other hand, PEO has terminal alcohol groups which can bind to the copper through removing the hydrogen group. The formation constants for Cu to PVP is approximately 10 in a tetra coordinate system while it is approximately 16 for Cu to PEO [83, 84]. As can be seen in the stability data, the PEO/Cu type complex is much stronger than that for the PVP/Cu and could account for the lower solubility observed in the current study.

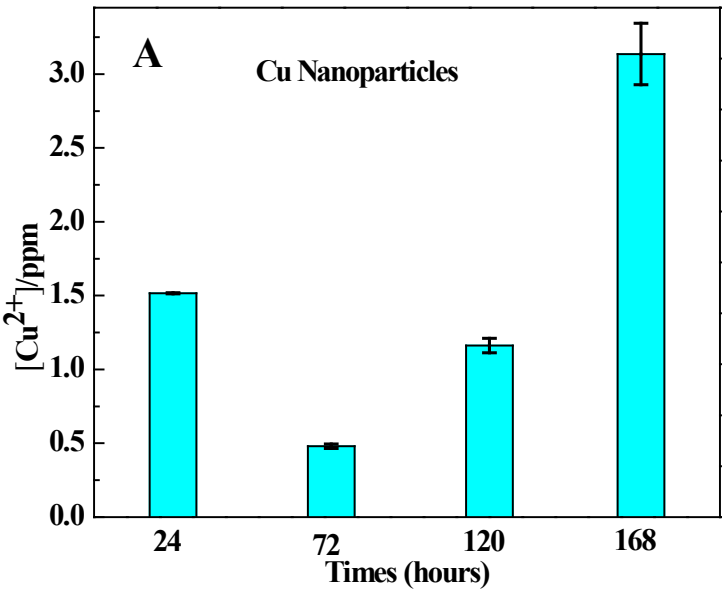


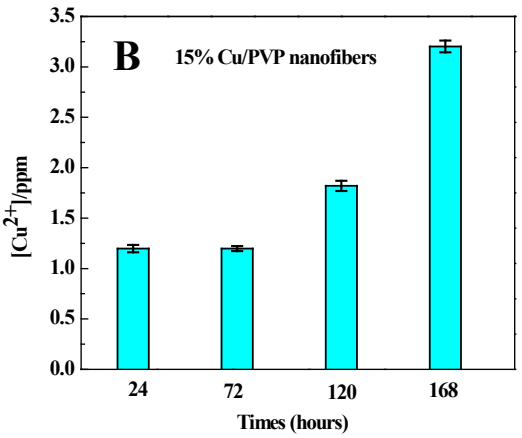


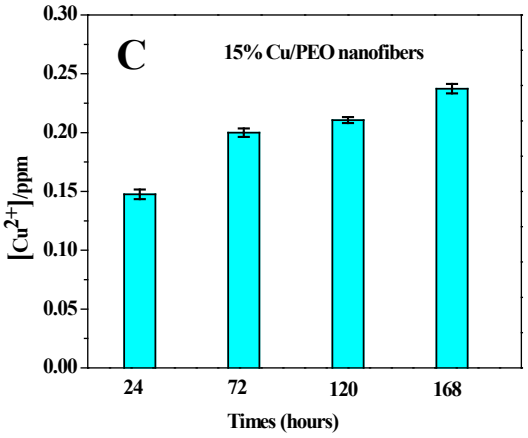

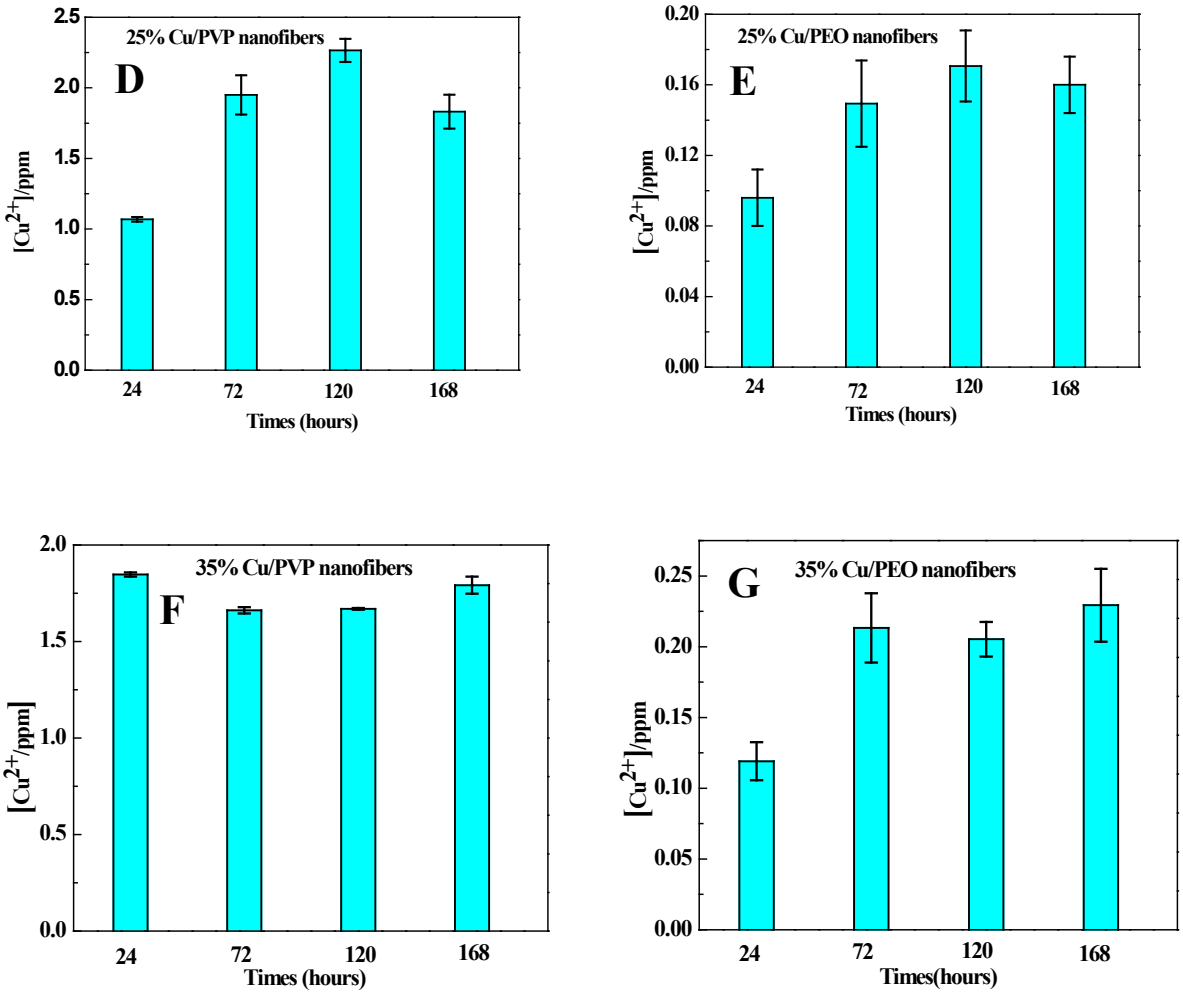


**Figure 7:** Concentration of $Cu^{2+}$ released from Cu NPs sample as a function of the immersion time. A figure is for $Cu^{2+}$ release. B, C indicating 15% $Cu^{2+}$ released from PVP/Cu and PEO/Cu fibers respectively. D, E indicates 25% $Cu^{2+}$ released from PVP/Cu and PEO/Cu fibers respectively. F, G indicates 35% $Cu^{2+}$ released from PVP/Cu and PEO/Cu fibers respectively.

## Conclusion

PEO/Cu and PVP/Cu composite fibers were fabricated by centrifugal spinning of PEO/Cu/Water and PVP/Cu/Ethanol precursor solutions, respectively. In this processing method, the spinneret speed (5500 rpm for PEO/Cu and 7000 rpm for PVP/Cu), favorable relative humidity (46%) and concentrations for both solutions (8 wt. % for PEO/Cu and 18 wt. % for PVP/Cu) were the interplay to obtain fine morphological fibrous mats. The structure and morphological characterization of the fibers were performed by SEM EDS, XRD which indicated the presence of distributed Cu nanoparticles throughout the nanofibrous membranes where 15, 25 and 35 wt. %

Cu NPs were vividly embedded in both composite fibers. For the antibacterial tests, a disk diffusion method was performed while inhibition zone for six samples (3 for each composite fibers) was detected accurately. During the Cu release study, Cu nanoparticles dissociate to $Cu^{2+}$ ion properly; assisting the microbial function of the nano-fibrous membrane to be implemented in bacterial cell effectively. For this reason, in agar plate medium, in case of gram-negative *E. coli*; the inhibition zone efficiency was near about 91.5 % for the both composite fibers at 35 wt. % concentration of Cu nanoparticles in the fiber-matrix. On the other hand, for gram positive bacteria *B. cereus*, 35 wt. % Cu concentration in both nanofiber samples showed 100 % inhibition efficiency. This was possible due to the high surface area to volume ratio based on which befitting Cu nanoparticles were dispersed into fibrous mats. Basically, centrifugally spun fibers were very porous in nature where Cu NPs can be capped very easily. In effect, more Cu nanoparticles were distributed on the surface of membranes and played a role to inactivate the bacterial cell membrane efficiently. Hopefully in future, both PEO/Cu and PVP/Cu nano-fibrous membranes could be a noticeable treatment from the exemption of the bacterial strains.

To the best of the authors' knowledge, this is the first results to be reported on the centrifugal spinning of Cu/PEO and Cu/PVP composite fibers for use as antibacterial agents against bacteria.

**Acknowledgment**

This work was also supported by National Science Foundation (NSF) PREM award under grant no. DMR- 2122178: UTRGV-UMN Partnership for Fostering Innovation by Bridging Excellence in Research and Student Success. Acknowledge the Bensen Endowment in Engineering. Partial support was provided by the Lloyd M. Bentsen, Jr. Endowed Chair in Engineering endowment at UTRGV.

***References***

[1] Z. Zhang, Y. Wu, Z. Wang, X. Zou, Y. Zhao, L. Sun, Fabrication of silver nanoparticles embedded into polyvinyl alcohol (Ag/PVA) composite nanofibrous films through electrospinning for antibacterial and surface-enhanced Raman scattering (SERS) activities, Materials Science and Engineering: C, 69 (2016) 462-469.

[2] M. Derrien, J.E. van Hylckama Vlieg, Fate, activity, and impact of ingested bacteria within the human gut microbiota, Trends in microbiology, 23 (2015) 354-366.
[3] J. Quirós, J.P. Borges, K. Boltes, I. Rodea-Palomares, R. Rosal, Antimicrobial electrospun silver-, copper- and zinc-doped polyvinylpyrrolidone nanofibers, Journal of hazardous materials, 299 (2015) 298-305.
[4] G. Broughton, II, J.E. Janis, C.E. Attinger, A Brief History of Wound Care, Plastic and Reconstructive Surgery, 117 (2006).
[5] K.M. Sawicka, P. Gouma, Electrospun composite nanofibers for functional applications, Journal of Nanoparticle Research, 8 (2006) 769-781.
[6] N.P. Desai, J.A. Hubbell, Surface modifications of polymeric biomaterials for reduced thrombogenicity, Proceedings of the ACS Division of Polymeric Materials: Science and Engineering, Publ by ACS, 1990, pp. 731-735.
[7] Q.P. Pham, U. Sharma, A.G. Mikos, Electrospinning of polymeric nanofibers for tissue engineering applications: a review, Tissue engineering, 12 (2006) 1197-1211.
[8] N. Khanam, C. Mikoryak, R.K. Draper, K.J. Balkus Jr, Electrospun linear polyethyleneimine scaffolds for cell growth, Acta biomaterialia, 3 (2007) 1050-1059.
[9] S. Kumbar, R. James, S. Nukavarapu, C. Laurencin, Electrospun nanofiber scaffolds: engineering soft tissues, Biomedical materials, 3 (2008) 034002.
[10] B.-M. Min, G. Lee, S.H. Kim, Y.S. Nam, T.S. Lee, W.H. Park, Electrospinning of silk fibroin nanofibers and its effect on the adhesion and spreading of normal human keratinocytes and fibroblasts in vitro, Biomaterials, 25 (2004) 1289-1297.
[11] M. Mattioli-Belmonte, A. Zizzi, G. Lucarini, F. Giantomassi, G. Biagini, G. Tucci, F. Orlando, M. Provinciali, F. Carezzi, P. Morganti, Chitin nanofibrils linked to chitosan glycolate as spray, gel, and gauze preparations for wound repair, Journal of Bioactive and Compatible Polymers, 22 (2007) 525-538.
[12] D.G. Castner, B.D. Ratner, Biomedical surface science: Foundations to frontiers, Surface Science, 500 (2002) 28-60.
[13] R. Rani, H. Kumar, R. Salar, S. Purewal, Antibacterial activity of copper oxide nanoparticles against gram negative bacterial strain synthesized by reverse micelle technique, Int. J. Pharm. Res. Dev, 6 (2014) 72-78.
[14] Š. Zupančič, L. Preem, J. Kristl, M. Putrinš, T. Tenson, P. Kocbek, K. Kogermann, Impact of PCL nanofiber mat structural properties on hydrophilic drug release and antibacterial activity on periodontal pathogens, European Journal of Pharmaceutical Sciences, 122 (2018) 347-358.
[15] J. Pelipenko, P. Kocbek, J. Kristl, Nanofiber diameter as a critical parameter affecting skin cell response, European Journal of Pharmaceutical Sciences, 66 (2015) 29-35.
[16] H. Matsumoto, A. Tanioka, Functionality in electrospun nanofibrous membranes based on fiber's size, surface area, and molecular orientation, Membranes, 1 (2011) 249-264.
[17] K. Balasubramanian, K.M. Kodam, Encapsulation of therapeutic lavender oil in an electrolyte assisted polyacrylonitrile nanofibres for antibacterial applications, Rsc Advances, 4 (2014) 54892-54901.
[18] K. Balasubramanian, R. Yadav, P. Prajith, Antibacterial nanofibers of polyoxymethylene/gold for pro-hygiene applications, International Journal of Plastics Technology, 19 (2015) 363-367.
[19] D. Pamfil, E. Butnaru, C. Vasile, Poly (vinyl alcohol)/chitosan cryogels as pH responsive ciprofloxacin carriers, Journal of Polymer Research, 23 (2016) 146.
[20] R.S. Ambekar, B. Kandasubramanian, A polydopamine-based platform for anti-cancer drug delivery, Biomaterials science, 7 (2019) 1776-1793.
[21] H. Liu, Y. Zhou, S. Chen, M. Bu, J. Xin, S. Li, Current sustained delivery strategies for the design of local neurotrophic factors in treatment of neurological disorders, asian journal of pharmaceutical sciences, 8 (2013) 269-277.
[22] Q. Liu, J. Huang, H. Shao, L. Song, Y. Zhang, Dual-factor loaded functional silk fibroin scaffolds for peripheral nerve regeneration with the aid of neovascularization, Rsc Advances, 6 (2016) 7683-7691.

[23] C. Huang, Y. Ouyang, H. Niu, N. He, Q. Ke, X. Jin, D. Li, J. Fang, W. Liu, C. Fan, Nerve guidance conduits from aligned nanofibers: improvement of nerve regeneration through longitudinal nanogrooves on a fiber surface, ACS applied materials & interfaces, 7 (2015) 7189-7196.
[24] M. Abrigo, S.L. McArthur, P. Kingshott, Electrospun nanofibers as dressings for chronic wound care: advances, challenges, and future prospects, Macromolecular bioscience, 14 (2014) 772-792.
[25] F.E. Ahmed, B.S. Lalia, R.J.D. Hashaikeh, A review on electrospinning for membrane fabrication: challenges and applications, 356 (2015) 15-30.
[26] X. Li, W. Chen, Q. Qian, H. Huang, Y. Chen, Z. Wang, Q. Chen, J. Yang, J. Li, Y.W.J.A.E.M. Mai, Electrospinning Techniques: Electrospinning-Based Strategies for Battery Materials (Adv. Energy Mater. 2/2021), 11 (2021) 2170010.
[27] V.A. Agubra, L. Zuniga, D. De la Garza, L. Gallegos, M. Pokhrel, M. Alcoutlabi, Forcespinning: A new method for the mass production of Sn/C composite nanofiber anodes for lithium ion batteries, Solid State Ionics, 286 (2016) 72-82.
[28] L. Zuniga, G. Gonzalez, R.O. Chavez, J.C. Myers, T.P. Lodge, M. Alcoutlabi, Centrifugally Spun alpha-Fe2O3/TiO2/Carbon Composite Fibers as Anode Materials for Lithium-Ion Batteries, Appl Sci-Basel, 9 (2019).
[29] L. Zuniga, V. Agubra, D. Flores, H. Campos, J. Villareal, M. Alcoutlabi, Multichannel hollow structure for improved electrochemical performance of TiO2/Carbon composite nanofibers as anodes for lithium ion batteries, J Alloy Compd, 686 (2016) 733-743.
[30] N. Obregon, V. Agubra, M. Pokhrel, H. Campos, D. Flores, D. De la Garza, Y.B. Mao, J. Macossay, M. Alcoutlabi, Effect of Polymer Concentration, Rotational Speed, and Solvent Mixture on Fiber Formation Using Forcespinning((R)), Fibers, 4 (2016).
[31] R.O. Chavez, T.P. Lodge, J. Huitron, M. Chipara, M. Alcoutlabi, Centrifugally spun carbon fibers prepared from aqueous poly(vinylpyrrolidone) solutions as binder-free anodes in lithium-ion batteries, J Appl Polym Sci, 138 (2021).
[32] D. De la Garza, F. De Santiago, L. Materon, M. Chipara, M. Alcoutlabi, Fabrication and characterization of centrifugally spun poly(acrylic acid) nanofibers, J Appl Polym Sci, 136 (2019).
[33] S.S.H. Abir, M.T. Hasan, M. Alcoutlabi, K. Lozano, The Effect of Solvent and Molecular Weight on the Morphology of Centrifugally Spun Poly(vinylpyrrolidone) Nanofibers, Fiber Polym, DOI 10.1007/s12221-021-1059-x(2021).
[34] J. Lopez, R. Gonzalez, J. Ayala, J. Cantu, A. Castillo, J. Parsons, J. Myers, T.P. Lodge, M. Alcoutlabi, Centrifugally spun TiO2/C composite fibers prepared from TiS2/PAN precursor fibers as binder-free anodes for LIBS, Journal of Physics and Chemistry of Solids, 149 (2021).
[35] A.S. Nain, M. Sitti, A. Jacobson, T. Kowalewski, C. Amon, Dry spinning based spinneret based tunable engineered parameters (STEP) technique for controlled and aligned deposition of polymeric nanofibers, Macromolecular rapid communications, 30 (2009) 1406-1412.
[36] J. Zhao, W. Han, H. Chen, M. Tu, R. Zeng, Y. Shi, Z. Cha, C. Zhou, Preparation, structure and crystallinity of chitosan nano-fibers by a solid–liquid phase separation technique, Carbohydrate polymers, 83 (2011) 1541-1546.
[37] D. Paneva, F. Bougard, N. Manolova, P. Dubois, I. Rashkov, Novel electrospun poly (ε-caprolactone)-based bicomponent nanofibers possessing surface enriched in tertiary amino groups, European Polymer Journal, 44 (2008) 566-578.
[38] S. Ramakrishna, An introduction to electrospinning and nanofibers, World Scientific2005.
[39] C. Saiyasombat, S. Maensiri, Fabrication, morphology, and structure of electrospun PAN-based carbon nanofibers, Journal of polymer engineering, 28 (2008) 5-18.
[40] T. Hou, X. Li, Y. Lu, B. Yang, Highly porous fibers prepared by centrifugal spinning, Materials & Design, 114 (2017) 303-311.

[41] R.O. Chavez, T.P. Lodge, M. Alcoutlabi, Recent developments in centrifugally spun composite fibers and their performance as anode materials for lithium-ion and sodium-ion batteries, Mater Sci Eng B-Adv, 266 (2021).
[42] M.T. Hasan, R. Gonzalez, M. Chipara, L. Materon, J. Parsons, M. Alcoutlabi, Antibacterial activities of centrifugally spun polyethylene oxide/silver composite nanofibers, Polym Advan Technol, 32 (2021) 2327-2338.
[43] J.L. Lumley, Drag reduction by additives, Annual review of fluid mechanics, 1 (1969) 367-384.
[44] S. Siggia, The chemistry of polyvinylpyrrolidone-iodine, Journal of the American Pharmaceutical Association (Scientific ed.), 46 (1957) 201-204.
[45] I. Iliopoulos, J. Halary, R. Audebert, Polymer complexes stabilized through hydrogen bonds. Influence of “structure defects” on complex formation: Viscometry and fluorescence polarization measurements, Journal of Polymer Science Part A: Polymer Chemistry, 26 (1988) 275-284.
[46] C.-l. Ren, R. Nap, I. Szleifer, The role of hydrogen bonding in tethered polymer layers, The Journal of Physical Chemistry B, 112 (2008) 16238-16248.
[47] N.P. Desai, J.A. Hubbell, Biological responses to polyethylene oxide modified polyethylene terephthalate surfaces, Journal of biomedical materials research, 25 (1991) 829-843.
[48] K.-H. Cho, J.-E. Park, T. Osaka, S.-G. Park, The study of antimicrobial activity and preservative effects of nanosilver ingredient, Electrochimica Acta, 51 (2005) 956-960.
[49] H. Savaş, O. Güven, Investigation of active substance release from poly (ethylene oxide) hydrogels, International journal of pharmaceutics, 224 (2001) 151-158.
[50] I. Kohsari, Z. Shariatinia, S.M. Pourmortazavi, Antibacterial electrospun chitosan–polyethylene oxide nanocomposite mats containing bioactive silver nanoparticles, Carbohydrate polymers, 140 (2016) 287-298.
[51] K.H. Jung, M.W. Huh, W. Meng, J. Yuan, S.H. Hyun, J.S. Bae, S.M. Hudson, I.K. Kang, Preparation and antibacterial activity of PET/chitosan nanofibrous mats using an electrospinning technique, Journal of Applied Polymer Science, 105 (2007) 2816-2823.
[52] S. Selvam, M. Sundrarajan, Functionalization of cotton fabric with PVP/ZnO nanoparticles for improved reactive dyeability and antibacterial activity, Carbohydrate polymers, 87 (2012) 1419-1424.
[53] F. Yalcinkaya, M. Komarek, D. Lubasova, F. Sanetrnik, J. Maryska, Preparation of antibacterial nanofibre/nanoparticle covered composite yarns, Journal of Nanomaterials, 2016 (2016).
[54] M. Karpuraranjith, S. Thambidurai, Chitosan/zinc oxide-polyvinylpyrrolidone (CS/ZnO-PVP) nanocomposite for better thermal and antibacterial activity, International journal of biological macromolecules, 104 (2017) 1753-1761.
[55] R. Bryaskova, D. Pencheva, S. Nikolov, T. Kantardjiev, Synthesis and comparative study on the antimicrobial activity of hybrid materials based on silver nanoparticles (AgNps) stabilized by polyvinylpyrrolidone (PVP), Journal of chemical biology, 4 (2011) 185.
[56] F. Yalcinkaya, D. Lubasova, Quantitative evaluation of antibacterial activities of nanoparticles (ZnO, TiO2, ZnO/TiO2, SnO2, CuO, ZrO2, and AgNO3) incorporated into polyvinyl butyral nanofibers, Polymers for Advanced Technologies, 28 (2017) 137-140.
[57] G. Ren, D. Hu, E.W. Cheng, M.A. Vargas-Reus, P. Reip, R.P. Allaker, Characterisation of copper oxide nanoparticles for antimicrobial applications, International journal of antimicrobial agents, 33 (2009) 587-590.
[58] J.P. Ruparelia, A.K. Chatterjee, S.P. Duttagupta, S. Mukherji, Strain specificity in antimicrobial activity of silver and copper nanoparticles, Acta biomaterialia, 4 (2008) 707-716.
[59] M. Gondwal, G. Joshi nee Pant, Synthesis and Catalytic and Biological Activities of Silver and Copper Nanoparticles Using Cassia occidentalis, International Journal of Biomaterials, 2018 (2018) 6735426.

[60] S.M. Briffa, I. Lynch, V. Trouillet, M. Bruns, D. Hapiuk, J. Liu, R. Palmer, E. Valsami-Jones, Development of scalable and versatile nanomaterial libraries for nanosafety studies: polyvinylpyrrolidone (PVP) capped metal oxide nanoparticles, RSC advances, 7 (2017) 3894-3906.
[61] M. Shahmiri, N.A. Ibrahim, F. Shayesteh, N. Asim, N. Motallebi, Preparation of PVP-coated copper oxide nanosheets as antibacterial and antifungal agents, Journal of Materials Research, 28 (2013) 3109.
[62] D. Flores, J. Villarreal, J. Lopez, M. Alcoutlabi, Production of carbon fibers through Forcespinning (R) for use as anode materials in sodium ion batteries, Mater Sci Eng B-Adv, 236 (2018) 70-75.
[63] M.R. Badrossamay, H.A. McIlwee, J.A. Goss, K.K. Parker, Nanofiber Assembly by Rotary Jet-Spinning, Nano Lett, 10 (2010) 2257-2261.
[64] S. Thenmozhi, N. Dharmaraj, K. Kadirvelu, H.Y. Kim, Electrospun nanofibers: New generation materials for advanced applications, Materials Science and Engineering: B, 217 (2017) 36-48.
[65] S. Padron, R. Patlan, J. Gutierrez, N. Santos, T. Eubanks, K. Lozano, Production and characterization of hybrid BEH-PPV/PEO conjugated polymer nanofibers by forcespinning (TM), J Appl Polym Sci, 125 (2012) 3610-3616.
[66] B.C. Weng, F.H. Xu, G. Garza, M. Alcoutlabi, A. Salinas, K. Lozano, The Production of Carbon Nanotube Reinforced Poly(vinyl) Butyral Nanofibers by the Forcespinning (R) Method, Polym Eng Sci, 55 (2015) 81-87.
[67] A. Hoffmann, A.J.C. Kuehne, High Throughput Centrifugal Electrospinning of Polyacrylonitrile Nanofibers for Carbon Fiber Nonwovens, Polymers-Basel, 13 (2021).
[68] S. Mei, X. Feng, Z. Jin, Polymer nanofibers by controllable infiltration of vapour swollen polymers into cylindrical nanopores, Soft Matter, 9 (2013) 945-951.
[69] R. Weitz, L. Harnau, S. Rauschenbach, M. Burghard, K. Kern, Polymer nanofibers via nozzle-free centrifugal spinning, Nano letters, 8 (2008) 1187-1191.
[70] Z.-M. Zhang, Y.-S. Duan, Q. Xu, B. Zhang, A review on nanofiber fabrication with the effect of high-speed centrifugal force field, Journal of Engineered Fibers and Fabrics, 14 (2019) 1558925019867517.
[71] Z. Li, S. Mei, Y. Dong, F. She, L. Kong, High efficiency fabrication of chitosan composite nanofibers with uniform morphology via centrifugal spinning, Polymers, 11 (2019) 1550.
[72] C. Liu, J. Sun, M. Shao, B. Yang, A comparison of centrifugally-spun and electrospun regenerated silk fibroin nanofiber structures and properties, Rsc Advances, 5 (2015) 98553-98558.
[73] K. Shameli, M.B. Ahmad, A. Zamanian, P. Sangpour, P. Shabanzadeh, Y. Abdollahi, M. Zargar, Green biosynthesis of silver nanoparticles using Curcuma longa tuber powder, International journal of nanomedicine, 7 (2012) 5603-5610.
[74] V. Bogatyrov, N. Borisenko, V. Pokrovskii, Thermal Degradation of Polyvinylpyrrolidone on the Surface of Pyrogenic Silica, Russian Journal of Applied Chemistry - RUSS J APPL CHEM-ENG TR, 74 (2001) 839-844.
[75] H.M. Ng, N. mohamad saidi, F.S. Omar, R. Kasi, R. T subramaniam, S. Baig, Thermogravimetric Analysis of Polymers, DOI 10.1002/0471440264.pst667(2018) 1-29.
[76] M. Polaskova, P. Peer, R. Cermak, P. Ponizil, Effect of thermal treatment on crystallinity of poly (ethylene oxide) electrospun fibers, Polymers, 11 (2019) 1384.
[77] J. Hou, Y. Wang, H. Xue, Y. Dou, Biomimetic growth of hydroxyapatite on electrospun CA/PVP core–shell nanofiber membranes, Polymers, 10 (2018) 1032.
[78] Y. Takahashi, H. Tadokoro, Structural Studies of Polyethers, (-(CH2)m-O-)n. X. Crystal Structure of Poly(ethylene oxide), Macromolecules, 6 (1973) 672-675.
[79] S. Åsbrink, L.-J. Norrby, A refinement of the crystal structure of copper (II) oxide with a discussion of some exceptional esd's, Acta Crystallographica Section B: Structural Crystallography and Crystal Chemistry, 26 (1970) 8-15.
[80] I.-K. Suh, H. Ohta, Y. Waseda, High-temperature thermal expansion of six metallic elements measured by dilatation method and X-ray diffraction, Journal of Materials Science, 23 (1988) 757-760.

[81] X.-f. Qian, J. Yin, S. Feng, S.-h. Liu, Z.-k. Zhu, Preparation and characterization of polyvinylpyrrolidone films containing silver sulfide nanoparticles, Journal of Materials Chemistry, 11 (2001) 2504-2506.
[82] S. Sriskandan, J. Cohen, Gram-positive sepsis: mechanisms and differences from gram-negative sepsis, Infectious disease clinics of North America, 13 (1999) 397-412.
[83] H. Nishikawa, E.J.T.J.o.P.C. Tsuchida, Complexation and form of poly (vinylpyridine) derivatives with copper (II) in aqueous solution, 79 (1975) 2072-2076.
[84] W.M. Hosny, P.A.J.I.J.E.S. Khalaf-Alaa, Potentiometric study and biological activity of some metal ion complexes of polyvinyl alcohol (PVA), 8 (2013) 1520-1533.